



HAL
open science

Short-term soil formation events in last glacial east European loess, evidence from multi-method luminescence dating

Daniel Veres, Viorica Tecsa, Natalia Gerasimenko, Christian Zeeden, Ulrich Hambach, Alida Timar-Gabor

► To cite this version:

Daniel Veres, Viorica Tecsa, Natalia Gerasimenko, Christian Zeeden, Ulrich Hambach, et al.. Short-term soil formation events in last glacial east European loess, evidence from multi-method luminescence dating. *Quaternary Science Reviews*, 2018, 200, pp.34-51. 10.1016/j.quascirev.2018.09.037 . hal-02319212

HAL Id: hal-02319212

<https://hal.science/hal-02319212>

Submitted on 28 Aug 2020

HAL is a multi-disciplinary open access archive for the deposit and dissemination of scientific research documents, whether they are published or not. The documents may come from teaching and research institutions in France or abroad, or from public or private research centers.

L'archive ouverte pluridisciplinaire **HAL**, est destinée au dépôt et à la diffusion de documents scientifiques de niveau recherche, publiés ou non, émanant des établissements d'enseignement et de recherche français ou étrangers, des laboratoires publics ou privés.



Distributed under a Creative Commons Attribution 4.0 International License



Short-term soil formation events in last glacial east European loess, evidence from multi-method luminescence dating

Daniel Veres^{a, b, *}, Viorica Tecsa^{b, c}, Natalia Gerasimenko^d, Christian Zeeden^e, Ulrich Hambach^f, Alida Timar-Gabor^{b, c, **}

^a Romanian Academy, Institute of Speleology, Clinicilor 5, 400006, Cluj-Napoca, Romania

^b Interdisciplinary Research Institute on Bio-Nano-Science of Babeş-Bolyai University, Treboniu Laurean 42, 400271, Cluj-Napoca, Romania

^c Faculty of Environmental Sciences and Engineering, Babeş-Bolyai University, Fântânele 30, 400294, Cluj-Napoca, Romania

^d Taras Shevchenko National University, Glushkova Prospect 2a, 03127, Kiev, Ukraine

^e IMCCE, Observatoire de Paris, PSL Research University, CNRS, Sorbonne Universités, UPMC Univ Paris 06, Univ Lille, 75014, Paris, France

^f BayCEER& Chair of Geomorphology, University of Bayreuth, D-95440, Bayreuth, Germany

ARTICLE INFO

Article history:

Received 28 March 2018

Received in revised form

18 September 2018

Accepted 26 September 2018

Available online 6 October 2018

Keywords:

Luminescence dating

Loess

MIS 2 embryonic soils

Climate dynamics

Eastern Europe

Millennial-scale loess records

Embryonic soils

Pleistocene

ABSTRACT

Here we provide a robust luminescence chronology for Stayky (Ukraine), a reference profile in European Late Pleistocene loess stratigraphy, based on optically stimulated luminescence (OSL) dating on quartz (4–11 μm , 63–90 μm) and post infrared-infrared stimulated luminescence (pIR-IRSL) on polymineral fine grains. For the Bug loess unit, the equivalent of Marine Isotope Stage (MIS 2), results are in agreement between methods, demonstrating that the suite of embryonic soils previously interpreted as reflecting climate variability similar to Greenland interstadials (GI) actually date to ~29/27–15 ka, with most emplaced around or after 20 ka. This temporal span is further confirmed by age-depth modelling of available data. Apart from GI-2, no interstadial-type climate events are recorded in Greenland ice core data for that time interval. As short-term pedogenetic phases are also documented in records from central-western Europe, there is a need for more research into the European mid-latitude terrestrial environments response to MIS 2 hydroclimate variability.

The dating of Vytachiv paleosol, previously debatably linked to various GI events within MIS 3 resulted in ages of -40 ± 4 ka and -53 ± 4 ka at the lower transition, and -26 ± 2 ka to -30 ± 2 ka in the overlying loess. These ages indicate that the truncated Vytachiv paleosol is either not continuous, or that it encompasses a broader age range within MIS 3 than previously considered. In both cases, data would not allow for an unambiguous linking of this paleosol with specific GI events as previously attempted.

The pIR-IRSL₂₉₀ dating of the loams immediately underneath Pryluky unit in the range of ~120 ka to ~168 ka and of the Pryluky mollisol from ~90 ka to 126 ka confirm the broad correspondence of this unit with MIS 5, although poor dose recovery results open the possibility for further testing on the degree these ages provide overestimated results. Quartz data severely underestimate the pIR-IRSL₂₉₀ ages for these samples. The application of pIR-IRSL₂₉₀ dating for the underlying Dnieper till previously linked to the Saalian glaciation resulted in natural signals at the level of laboratory saturation, yielding minimum ages of c. 700 ka. For the same sample, the natural SAR-OSL signals for 4–11 μm quartz were found significantly below laboratory saturation level, resulting in finite ages of ~250–270 ka interpreted here as underestimates, while coarse quartz (63–90 μm) signals reached about 85% of the laboratory saturation level. These data suggest extreme caution must be taken when dating such old samples using quartz OSL. Results from our high-resolution luminescence dating raises important implications for the chronological representativeness of Stayky as a key loess site in Eastern Europe beyond MIS 2.

© 2018 The Authors. Published by Elsevier Ltd. This is an open access article under the CC BY-NC-ND license (<http://creativecommons.org/licenses/by-nc-nd/4.0/>).

* Corresponding author. Interdisciplinary Research Institute on Bio-Nano-Science of Babeş-Bolyai University, Treboniu Laurean 42, 400271, Cluj-Napoca, Romania.

** Corresponding author. Interdisciplinary Research Institute on Bio-Nano-Science of Babeş-Bolyai University, Treboniu Laurean 42, 400271, Cluj-Napoca, Romania.

E-mail addresses: daniel.veres@ubbcluj.ro (D. Veres), alida.timar@ubbcluj.ro (A. Timar-Gabor).

1. Introduction

Loess-paleosol sequences (LPS), as some of the most spatially spread terrestrial deposits, provide crucial insights into past

environmental dynamics, particularly where other long-term paleoclimate data are scarce (Kukla, 1977; Heller and Liu, 1982; Vandenberghe, 2000; Panaiotu et al., 2001; Guo et al., 2002; Lindner et al., 2006; Buggle et al., 2008, 2013; Haesaerts et al., 2010; Kusiak et al., 2012; Jary and Ciszek, 2013; Obreht et al., 2016; Zeeden et al., 2016; Gozhik et al., 2014; Marković et al., 2011, 2015). Owing to the nature of their formation (Sprafke and Obreht, 2016), the LPS are valuable in investigating past variability in atmospheric particle loading (Ruth et al., 2007; Bokhorst et al., 2011; Rousseau et al., 2017a; b) and long-term global dust dynamics (Kohfeld, 2003; Delmonte et al., 2004; Újvári et al., 2016a). As the primary constituent of loess, mineral dust is a major component of global climate forcing (Maher et al., 2010; Sima et al., 2013; Újvári et al., 2016a; Longman et al., 2017) and a proxy that has allowed for direct comparison of LPS with chronologically better resolved ice and marine records (Evans et al., 2003; Svensson et al., 2008; Veres et al., 2013a; Rasmussen et al., 2014; Rousseau et al., 2007, 2011; 2017a; b; Moine et al., 2017).

Investigations of Eurasian LPS document a pattern with mainly, if not only well-developed major paleosols interbedded with thick loess horizons (Ding et al., 2002; Guo et al., 2002; Hao et al., 2012; Buggle et al., 2008, 2013; Marković et al., 2011, 2015; Fitzsimmons et al., 2012; Zech et al., 2013; Zeeden et al., 2016). These records have been linked to orbital forcing driving glacial-interglacial cycles (cf., Heller and Liu, 1982; Lisiecki and Raymo, 2005; Lang and Wolff, 2011), with major paleosols formed during interglacials and loess horizons representing stadial conditions with enhanced global dust cycling (Marković et al., 2015 and references therein).

Overall, reliable chronological control is still the major limiting factor in exploring the full paleoclimate potential of LPS (Vandenberghe, 2000; Hao et al., 2012; Basarin et al., 2014; Marković et al., 2011, 2015; Obreht et al., 2016; Zeeden et al., 2018a; b). Moreover, mainly along mid-latitudes in Eurasia or along major river valleys, incipient (or embryonic) soils have been described within the last glacial loess or loess-derivates (Vandenberghe et al., 1998; Haesaerts and Mesdagh, 2000; Antoine et al., 2001, 2013; Gerasimenko, 2006; Haesaerts et al., 2010, 2016; Rousseau et al., 2001, 2011; Bokhorst et al., 2011; Fuchs et al., 2013; Jary and Ciszek, 2013; Meszner et al., 2013; Terhorst et al., 2014; Lehmkuhl et al., 2016). Such short-term phases of pedogenesis have been regarded as likely equivalents of Greenland interstadials (GI) (Rousseau et al., 2011, 2017a; b; Moine et al., 2017) and linked to rapid changes in moisture availability (Antoine et al., 2001; Gerasimenko, 2006; Rousseau et al., 2011). As millennial-scale climate variability is well expressed in paleoclimate records from within the European loess belt as periods of enhanced/diminished organic productivity and biomass development (Caspers and Freund, 2001; Ampel et al., 2008; Wohlfarth et al., 2008; Fleitmann et al., 2009; Veres et al., 2009; Sanchez Goñi and Harrison, 2010; Fletcher et al., 2010; Shumilovskikh et al., 2014; Magyari et al., 2014; Sirocko et al., 2016), it is reasonable to assume that even short-term enhanced ground moisture sustaining biomass growth should be reflected in loess records as well. On the contrary, the typical loess plateaus of southeastern Europe were regarded as too dry for sustaining short-term phases of pedogenesis (Buggle et al., 2013; Marković et al., 2015); recent works proved however that MIS 3 millennial-scale climate variability is discernible in moisture and weathering proxies (Hatté et al., 2013; Obreht et al., 2017; Zeeden et al., 2018).

Major questions that require further research concern the temporal and spatial development of such embryonic soils (Labaz et al., 2018) and their regional representation in pedostratigraphic terms (Bábek et al., 2011; Gocke et al., 2014; Łanczont et al., 2014). Lateral changes in geological and geomorphological characteristics (Stevens et al., 2011; Antoine et al., 2013; Kadereit et al., 2013;

Meszner et al., 2013; Terhorst et al., 2014; Vandenberghe et al., 1998, 2014; Lehmkuhl et al., 2016; Fischer et al., 2018), or local to regional periodic shifts in hydroclimate conditions (Bokhorst et al., 2011; Buggle et al., 2013; Hatté et al., 2013; Sima et al., 2013; Zech et al., 2013; Hošek et al., 2015; Obreht et al., 2016, 2017) further complicate the validity of regional pedostratigraphic relationships (see Marković et al., 2015 and references therein). This includes the correlation of paleoclimate events among LPS records and with other paleoclimate archives (Evans et al., 2003; Shi et al., 2003; Maher et al., 2010; Újvári et al., 2016b; Fitzsimmons et al., 2012; Basarin et al., 2014; Zeeden et al., 2018a; Kadereit and Wagner, 2014; Govin et al., 2015; Rousseau et al., 2007, 2017a; b; Sauer et al., 2016; Moine et al., 2017). These issues are even more compelling when considering the role LPS might play in disentangling regional or even hemispheric past climate scenarios if considered within a larger and widely applicable chronostratigraphic framework (Sima et al., 2013; Govin et al., 2015; Moine et al., 2017; Obreht et al., 2017; Rousseau et al., 2017a; b).

In northern Ukraine at Stayky LPS (Fig. 1a–b) a record of past rapid climate variability expressed as the alternation of loess beds and several thin, incipient or embryonic soils has been documented within the Bug loess unit (Fig. 1c–d) (Gerasimenko, 2006; Gerasimenko and Rousseau, 2008; Rousseau et al., 2011). On these grounds, Stayky is considered an important record for exploring environmental dynamics during the last glacial period in eastern Europe (Rousseau et al., 2011, 2017a; b; Sima et al., 2013; Moine et al., 2017). However, because of insufficient dating (Rousseau et al., 2011), the proposed chronological setting and correlation of embryonic soils with Greenland Interstadial (GI) events has been questioned by Kadereit and Wagner (2014).

To date, luminescence techniques remain the main methods in providing radiometric data for loess following their applicability in directly dating the emplacement time of mineral particles (Roberts, 2008). In recent years, chronological and methodological advances have been achieved in the luminescence dating of eastern European LPS (Balescu et al., 2003; Stevens et al., 2011; Timar et al., 2010; Vasiliuic et al., 2012, 2013; Constantin et al., 2014). This includes comparisons of luminescence with tephrochronology or radio-carbon dating (Constantin et al., 2012; Fitzsimmons et al., 2013; Veres et al., 2013b; Anecitei-Deacu et al., 2014; Gozhik et al., 2014; Trandafir et al., 2015; Újvári et al., 2016b) and correlative age models (Obreht et al., 2017; Zeeden et al., 2018). However, issues linked to the grain size dependency of saturation characteristics and uncertainties induced by varying water contents (Timar-Gabor et al., 2011, 2012; 2015, 2017; Timar-Gabor and Wintle, 2013) still limit the application of luminescence data in age-depth modelling (Blaauw et al., 2010; Stevens et al., 2011; Újvári et al., 2016b; Zeeden et al., 2018b), precluding a secure identification of past climate events in loess records.

In order to substantiate the chronology of Stayky LPS, results of multi-method luminescence investigations of fifteen samples (Fig. 1d–e) are reported. State of the art optically stimulated luminescence (OSL) dating has been applied on all samples, alongside post infrared-infrared stimulated luminescence (pIR-IRSL) dating. Each sample has been dated using different grain-sizes and water content assessments; the results allow for a more comprehensive chronological overview of the Stayky sequence than previously achieved.

2. Regional chronostratigraphic considerations and issues

In the Ukrainian Quaternary chronostratigraphic framework (Veklich, 1993), six units were established above the Dnieper (Saalian) glaciogenic deposits. Two correlation schemes with MIS stages are in use. In the first, the Dnieper (dn) unit is the equivalent

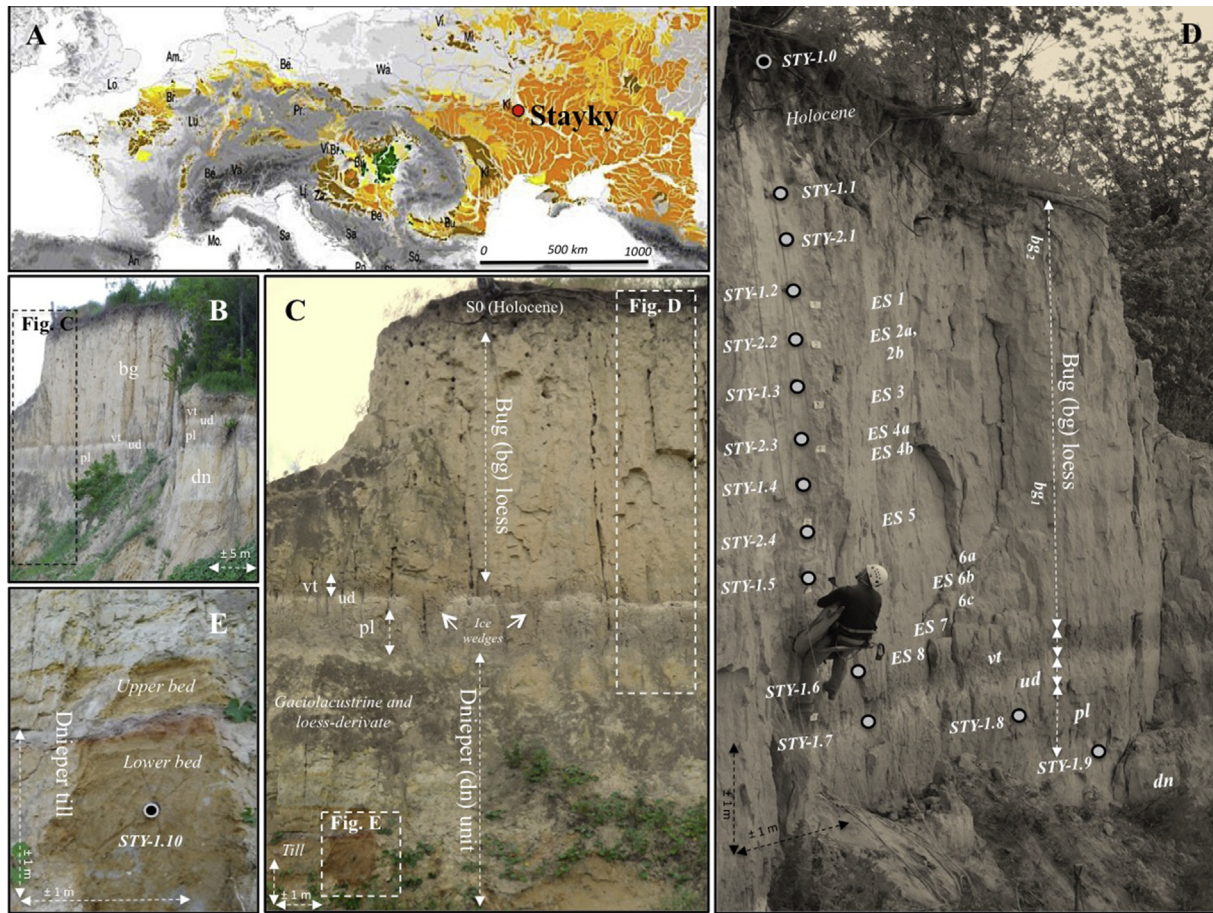


Fig. 1. Schematic representation of loess distribution in Europe (adapted from Haase et al., 2007) and location of Stayky in eastern Europe (a); The loess-paleosol profile at N-Stayky section near Kiev, northern Ukraine (b); Close-up view of the N-Stayky loess-paleosol profile, and distribution of main lithostratigraphic units discussed in the text (c); The down-wall distribution of OSL samples in relation to the embryonic soils (ES) and other chronostratigraphic units discussed in the text. The height of the sampled sequence is around 10 m (d); Close-up image of the Dnieper till and the location of sample STY-1.10 (e). Colour visualisation of this figure is available in the web version of the article. (For interpretation of the references to colour in this figure legend, the reader is referred to the Web version of this article.)

of MIS 8, Kaydaky (kd) soil unit of MIS 7, Tyasmyn (ts) loess unit of MIS 6, Pryluky (pl) pedocomplex of MIS 5 (Veklich, 1993; Lindner et al., 2006; Gozhik et al., 2014). This correlation relies mainly on the number of paleosols recognizable above the Dnieper till and radiometric data. Alternatively, the Dnieper unit is correlated with MIS 6 instead, whereas Kaydaky, Tyasmyn and Pryluky units were linked to MIS 5e, 5d and 5c-a (Rousseau et al., 2001; Gerasimenko, 2006; Buggle et al., 2008, 2009; Matviishina et al., 2010; Bokhorst et al., 2011; Haesaerts et al., 2010, 2016). This is based on long-range pedostratigraphic correlations with central-western European records, and further constrained by the interglacial-type pollen succession documented for the Kaydaky paleosol at Vyazivok (Rousseau et al., 2001), the stratotype of the Ukrainian Quaternary within the formerly glaciated upper-middle Dnieper basin. The correlation of the upper units is similar for both schemes: Uday (ud) unit is linked to MIS 4, Vytachiv (vt) pedocomplex to MIS 3, and Bug (bg) unit corresponds to MIS 2, whereas the Holocene chernozem represents MIS 1.

In the Kyiv loess plain where Stayky is located (Fig. 1a) most chronostratigraphic units can be traced laterally over large areas albeit significant variations in thickness and sedimentological characteristics (Veklich et al., 1984; Matoshko, 1999; Gerasimenko, 2006; Gerasimenko and Rousseau, 2008; Karmazinenko, 2010). Stayky comprises from top to bottom the Holocene chernozem, Bug loess, Vytachiv paleosol, Uday loess, Pryluky pedocomplex

(Veklich, 1968). The Kaydaky grey forest soil is preserved only in places, whereas the Tyasmyn loess bed is missing. The Dnieper unit comprises loess, glaciolacustrine loams and till, the latter overlying either glaciolacustrine loams, or truncated Middle and even Lower Pleistocene paleosols (Veklich et al., 1984; Matoshko, 1999).

Two main profiles have been studied at Stayky, located in different quarries. Detailed paleopedological, palynological and malacological studies (Veklich et al., 1984; Kunitsa, 2007) were conducted for the southern profile (S-Stayky), where the Vytachiv paleosol identified there was related to the lower brown forest soil of the Vytachiv pedocomplex in other sites. The Pryluky unit was regarded as a welded paleosol with a thick chernozem overlain by a thin brown soil. In former depressions, the Bt horizon of a forest soil (supposedly the Kaydaky paleosol) underlay this chernozem. Palynological data (Veklich et al., 1984) indicate cold forest-steppe with xerophytic herbs and some boreal trees for the Bug, Uday and Dnieper units. Pollen from the Vytachiv unit indicated pine forests with admixtures of spruce and broad-leaved trees, whereas a temperate forest-steppe has been inferred for Pryluky unit.

In a multi-proxy study of the Stayky northern quarry sequence (N-Stayky), the Dnieper unit was correlated with MIS 6 and the onset of last glacial cycle linked with Pryluky unit comprising a mollisol (chernozem) overlain by a truncated cambisol, both dissected by root tracks and frost wedges (Rousseau et al., 2011). The Vytachiv unit overlying the thin Uday loess bed (Fig. 1b–d)

shows the highest values in magnetic susceptibility, thus reflecting a phase of enhanced pedogenesis (Rousseau et al., 2011). The Bug (bg) loess unit in the Kyiv area has been studied in detail through pollen, grain-size and geochemical analyses (Gerasimenko, 2006). That study discussed also a series of four embryonic soils (ES) separated by and encompassed into loess beds pertaining to the bg_1 loess subunit. Later, Gerasimenko and Rousseau (2008) identified six ES at N-Stayky, whereas Rousseau et al. (2011) further reported on twelve distinct ES within the Bug loess at the same site (Fig. 1d). Higher organic carbon contents in ES have been interpreted as reflecting short-term increases in moisture (and thus biomass development accompanied by pedogenesis), and depletion in dust deposition during their formation (Gerasimenko, 2006; Rousseau et al., 2011). Pollen data also demonstrate a quasi-cyclic pattern with predominantly boreal taxa in ES, and arctic-alpine species in loess. Following a decrease in clay content from Pryluky unit to the lowermost ES, a cyclic pattern in coarse silt distribution has been inferred and linked to rapid shifts in regional atmospheric circulation patterns, moisture availability, and dust cycling (Rousseau et al., 2011, 2017a; b; Sima et al., 2013). A mineralogical investigation of the Bug loess indicated the prevalence of westerly winds during its accumulation (Chlebovsky et al., 2003). Further, a correlation of N-Stayky with Nussloch (Antoine et al., 2001) has been proposed, that in turn allowed for a comparison with Greenland ice mineral dust record (Rousseau et al., 2011, 2017a; b; Sima et al., 2013; Moine et al., 2017). Thus, the Vytachiv cambisol (IRSL age of 30.2 ± 3.1 ka) has been correlated with Greenland Interstadial (GI-) 8, the first strong increase in grain-size index (prior to the IRSL age of 27.6 ± 2.7 ka) corresponds to Heinrich event (H) 3 and its maximum increase (after 27.6 ± 2.7 ka) was linked to H2 (Rousseau et al., 2011). Following Rousseau et al. (2011; 2017a,b), the close correlation between Nussloch and Stayky highlights the environmental impact that North Atlantic abrupt climatic variability had on the terrestrial environments in mid-latitude Europe on a millennial-to-centennial time-scale during MIS 3. The overall chronological scenario was however questioned by Kadereit and Wagner (2014) who suggested that the temporal span of the LPS at Stayky is likely younger, with the Vytachiv paleosol linked to GI-7 or even GI-5, and that the twelve embryonic soils within the Bug loess unit likely postdate H2.

3. Materials and methods

3.1. The N-Stayky profile and sample collection

The N-Stayky LPS is situated on the right bank of Dnieper river, south of Kyiv ($50^{\circ}05.65' N$, $30^{\circ}53.92' E$, 194 m a.s.l.) (Fig. 1a–b). The profile is around 15 m thick, and for luminescence dating, fifteen samples were collected in 6-cm wide and 10-cm long steel tubes from a section parallel to that of Rousseau et al. (2011) (Fig. 1c–e). Due to loess wall collapse, the two sections could differ slightly, but the stratigraphy from Pryluky unit to the top is very similar (Fig. 1b–d). Therefore, we closely follow the profile description in Rousseau et al. (2011), augmented by our own stratigraphic observations.

The topmost *Holocene* mollisol (chernozem) is 1.3 m thick and clearly separated into genetic horizons. The A1 horizon comprises a dark-grey silty loam, porous, loose, with granular structure and gradual transition into the lighter brownish-grey A1-Bca horizon with carbonate punctuation and a distinctly undulating lower boundary. The Bca horizon is greyish-brown, with crumbly structure, small carbonate nodules, and strongly bioturbated. The Cca horizon comprises whitish-yellow carbonate impregnated coarse silts. Sample STY-1.0 was collected from 37 cm depth; due to strong bioturbation, the lower half of the topsoil, as well as the underlying

loess down to 1.7 m from top were not sampled.

The Bug (*bg*) unit comprises two distinct sub-units. Pale-yellow loose loess, porous, bioturbated with rootlets filled with carbonates and humus forms the bg_2 subunit (1.30–2.82 m). The lower subunit (bg_1) shows a cyclic alternation of thin embryonic soils (ES) interbedded within loess. The uppermost ES1 (2.82–2.92 m) differs from the encompassing loess by a slightly dark brownish tint and a noticeable decrease in carbonates. The underlying gleyed bluish-grey loess (2.92–3.10 m) is rich in carbonates but also in iron hydroxides indicating water logging (Rousseau et al., 2011). ES2a (3.10–3.17 m) is light brown and underlain by slightly gleyed loess, whereas ES2b (3.43–3.60 m) is darker and thicker than ES1 or ES2a, with distinct boundaries and less carbonate; the underlying loess (3.60–3.92 m) is enriched in carbonates. ES3 (3.92–4.20 m) is dissected by thin vertical cracks filled with loess and underlain by carbonate-impregnated loess (4.20–4.40 m). ES4 is greyish in colour and bipartite comprising two weak soil horizons at 4.40–4.60 m and 4.65–4.82 m, with the underlying whitish loess representing the Cca horizon of this soil couplet. ES5 (5.20–5.60 m) is the strongest developed among the embryonic soils, comprising the A1, B and BC horizons, whereas the Cca horizon in the underlying loess (5.60–5.80 m) is completely impregnated with carbonates. The tri-partite ES6 is light brown, with a cumulate thickness of around 60 cm (5.80–6.40 m) (Rousseau et al., 2011). ES7 (6.50–6.78 m) is dark greyish-brown with black punctuations by manganese hydroxides and a distinct transition towards the weakly expressed Cca horizon (6.78–6.83 m). The lowermost embryonic soil ES8 (6.83–7.0 m) is dark grey and richer in fine silt compared to other embryonic soils, with a distinctly undulating lower boundary (Rousseau et al., 2011). The thin loess bed (7.0–7.10/7.20 m) that separates it from the Vytachiv paleosol is pale-yellow, loose, porous and composed of rather fine silt (Rousseau et al., 2011) with a sharp and undulated lower boundary. Ten luminescence samples were collected from the Bug unit (Fig. 1d).

The Vytachiv unit (7.10/7.20–7.60 m) is represented by a greyish-brown fine-silt to clayey cambisol, with weak prismatic structure and a distinctively whitish Cca horizon. Its lower boundary is disturbed by cryostructures including long soil 'tongues' and wide shallow soil wedges, regularly distributed (Rousseau et al., 2011). Samples STY-1.6 and STY-1.7 roughly bracket the Vytachiv unit and the transition to the overlying Bug loess (Fig. 1d). The underlying Uday unit comprises only a thin (7.60–7.90/8.0 m) loess-like material, enriched in fine silt and clay, porous, with carbonate impregnations towards the top and partially laminated. Both upper and lower transitions are sharp and uneven, presumably erosional.

The Pryluky (*pl*) unit (Fig. 1d) forms a pedocomplex (8.0–9.20/9.30 m), with the uppermost light-brown truncated cambisol (0.2–0.3 m thick), enriched in clay, with weak prismatic structure and loose carbonates in the Cca horizon (Fig. 1c). The soil material is preserved also in long and thin fissures and pot-like cryostructures, which deform the underlying mollisol (Rousseau et al., 2011). As loess has been described within the cryostructures, it is likely that the cryogenic phase occurred after the cambisol was formed. The mollisol comprises a thick (up to 0.85 m) dark-grey A1 horizon and a thinner (0.2–0.3 m) light brownish-grey BCca horizon. The latter is structureless, loose and carbonate-rich, whereas large krotovinas filled with humus material occur frequently. The A1 horizon is carbonate-free, granular, loose and richer in coarse silt as compared to the cambisol (Rousseau et al., 2011). Its lower boundary is deformed by up to 1 m long soil wedges. These features point to a strong cryoturbation phase between the two soil horizons. The accumulation of a thin loess bed during this interval has been documented elsewhere in the area (Rousseau et al., 2001; Gerasimenko, 2006; Haesaerts et al., 2016). Sample STY-1.8 has

been collected from the upper part of Pryluky mollisol (Fig. 1d), whereas STY-1.9 was sampled just below the transition between the mollisol and an ochre-gley hydromorphic loess-like material with soil aggregates (9.25–9.85/10.0 m), bright bluish fillings of multiple vertical root channels, and a weak prismatic structure. It is not yet clear whether this unit represents the equivalent of Kaydaky paleosol (Karmazinenko, 2010), or just loess overprinted by hydromorphism and soil development. Its lower transition is gradual and in places uneven.

The Dnieper (*dn*) unit comprises beds of different lithology and sedimentological characteristics (Fig. 1b–e). Light bluish-grey sandy silts, finely bedded, with a very sharp lower boundary and small-scale silty intrusions into the underlying till form the upper glaciolacustrine deposits (10.0–10.8 m). The till (visible thickness up to 4 m) comprises mainly reddish-brown sandy loams rich in erratics (Veklich, 1968). Its upper part (1–2.5 m thick) includes multiple lenses of black soil material supposedly from Middle and Lower Pleistocene vertisols, and locally, stripes of a dark red-brown soil material. These till beds are separated by either ochre-white sands (20–30 cm thick), or by a clearly defined couplet of dark bluish-grey and red-brown clayey silts (Fig. 1d). This couplet is traced in other sections comprising the Dnieper till, documenting a laterally continuous sedimentation pattern within the Dnieper unit in this area (Gerasimenko, 2006). Sample STY-1.10 has been collected from the Dnieper till (Fig. 1d).

3.2. Luminescence dating

3.2.1. Preparation of luminescence samples

Sample preparation for luminescence dating was performed in the laboratory under low intensity red light conditions using standard procedures described in detail in the Supplementary File. For quartz analysis, the purity of extracts was evaluated using the infrared stimulated luminescence (IRSL) response to a regenerative β -dose. A significant sensitivity to infrared stimulation accounts for an IR depletion ratio deviating more than 10% from unity (Duller, 2003). Moreover, the high purity of quartz extracts has been confirmed by scanning electron microscopy (SEM) and chemical analysis of local area by energy dispersive X-ray spectroscopy (EDX) using a FEI Quanta 3D FEG dual beam microscope. Such data are presented for two samples, STY-1.0 collected from the Holocene soil and STY-1.1 collected from the Bug (*bg*₂) loess (Fig. 1d) (see Supplementary File Fig. S1). For both samples, other elements except O and Si (Al for STY-1.0 and Al, Na, Mg for STY-1.1) make up only 0.2% and 1.1%, respectively. It can therefore be stated that the extracts are very clean, consisting almost exclusively of quartz and that any muscovite or feldspars contamination is negligible.

3.2.2. Optically stimulated luminescence (OSL) and post infrared infrared stimulated luminescence (pIR-IRSL) measurements

Luminescence measurements were performed using an automated Risø TL/OSL-DA-20 reader, equipped with blue and infrared light diodes emitting at 470 ± 30 nm and 875 ± 80 nm, respectively. The emitted luminescence signals were detected by an EMI 9235QA photomultiplier tube (Thomsen et al., 2006). Irradiation of the samples was performed using the incorporated ^{90}Sr – ^{90}Y beta source, and further calibrated using standard gamma-irradiated calibration quartz produced by Risø National Laboratory, Denmark (Hansen et al., 2015). The dose rate for coarse quartz grains mounted on stainless steel disks was 0.138 Gy/s, whereas the dose rate for the fine grains mounted on aluminium disks was 0.115 Gy/s at the time of measurement.

Optically stimulated luminescence investigations were carried out on fine (4–11 μm) and coarse (63–90 μm ; 180–250 μm) quartz

using the single-aliquot regenerative dose (SAR) protocol (Murray and Wintle, 2000, 2003; Wintle and Murray, 2006). Stimulation of the luminescence signals with the blue light emitting diodes was maintained for 40 s at 125 °C, while the signals were recorded through a 7.5 mm thick Hoya U-340 UV filter. The net continuous wave optically stimulated luminescence (CW-OSL) signal was evaluated from the first 0.308 s of the decay curve with an early background subtraction (Cunningham and Wallinga, 2010) assessed from the 1.69–2.30 s interval. A preheat temperature of 220 °C for 10 s and a cutheat to 180 °C were employed throughout the SAR protocol unless otherwise stated. The OSL response to a fixed test dose of 17 Gy was used throughout the whole set of measurements to correct for sensitivity changes. At the end of each SAR cycle, a high-temperature bleach for 40 s at 280 °C was performed by stimulation with blue diodes (Murray and Wintle, 2003).

Equivalent doses for polymineral fine 4–11 μm grains were determined using the post infrared-infrared stimulated luminescence pIR-IRSL₂₉₀ protocol (Thiel et al., 2011a; Buylaert et al., 2011b, 2012). After a preheat of 320 °C for 60 s, the aliquots were stimulated with IR diodes for 200 s while held at 50 °C in order to recombine the near-neighbour trap/centre pairs which are prone to fading. Subsequent IR stimulation (200 s) was performed at 290 °C (pIR-IRSL₂₉₀); the dating signal of interest was recorded during this period. Natural, regenerative and test-dose response were all measured using the same preheat. Prior to proceeding to the next measurement cycle, any remaining signal was removed by infrared illumination at 325 °C for 100 s. Within each run both the pIR-IRSL₂₉₀ and the IR₅₀ signals were recorded. Thus, data for this IR₅₀ signal were obtained and are further presented (Table 1 and Supplementary File Table S2). The IRSL signals from polymineral fine grains, both at 50 °C and 290 °C, were detected through a blue filter combination (Schott BG39 + Corning 7–59, with transmission in the range of 320–460 nm). The IRSL signals were derived from the initial 2.5 s of the decay curve minus a background calculated using the last 50 s of stimulation.

The multi-elevated-temperature pIR-IRSL (MET-pIRIR) protocol (Li and Li, 2011) was also applied on a selection of polymineral fine grain samples (STY-2.4, STY-1.8 and STY 1.9). In this protocol a preheat temperature of 300 °C for 10 s was applied after both regenerative and test doses. After the preheat, MET-pIRIR signals of both regenerative and test doses are measured by increasing the stimulation temperature in steps of 50 °C. Prior to proceeding to the next measurement cycle, IR bleach at 320 °C for 100 s is conducted to ensure a low residual of IRSL signal for the next cycle. Signal integration and background correction was performed as described for the pIR-IRSL₂₉₀ protocol. The modified version of the MET-pIRIR protocol suggested by Fu and Li (2013) that implies the preheat to 200 °C coupled with repeated stimulation in steps of 30 °C up to 170 °C for 100 s was further applied on sample STY-1.0 collected from the Holocene soil.

3.2.3. Dose rate determination

The specific activities of radionuclides (^{238}U , ^{232}Th , ^{40}K) were measured by high-resolution gamma spectrometry. Measurements were performed twice using two high purity Ge detectors namely an ORTEC GMX HPGe detector with a width at half maximum (FWHM) of 1.92 keV at 1.33 MeV and a 0.5 mm Be window, further referred to as 'planar detector' and on a coaxial detector with hyperpure germanium well detector with a volume of 120 cm³, full width at half maximum (FWHM) at 122 KeV of 1.40 KeV and a full width at half maximum (FWHM) at 1332 KeV of 2.30 KeV, further denoted as 'well detector'. Relative calibrations were performed using the IAEA 312 and IAEA 327 standards. Results of the comparison between the two detectors are presented in Supplementary File Table S1, while ages obtained using data from different

Table 1

Summary of the IRSL at 50 °C, pIR-IRSL₂₉₀ and OSL ages obtained on polymineral fine (4–11 µm) grains, fine (4–11 µm) and coarse (63–90 µm) quartz and the dosimetry data. The ages for IRSL at 50 °C as well as pIR-IRSL at 290 °C are not corrected for anomalous fading. The uncertainties associated with the luminescence and dosimetry data are random; the uncertainties mentioned with the optical ages are the overall uncertainties. *n* denotes the number of accepted aliquots; the systematic errors taken into account for calculating the total errors on the ages include relative errors of: 2% beta source calibration, 3% conversion factors, 5% attenuation and etching factors, 3% gamma spectrometer calibration, 15% cosmic radiation, 25% water content, 50% alpha efficiency values. All uncertainties represent 1σ. Specific activities were measured on Well detector and the ages were determined considering the “measured water” content as well as assumed water content of 15%; beta attenuation and etching factor used for 63–90 µm quartz was 0.94 (Mejdahl, 1979); adopted alpha efficiency factor was 0.04 for 4–11 µm quartz and 0.08 for polymineral 4–11 µm fine-grains, respectively (Rees-Jones, 1995). The total dose rate consists of the contribution from the beta and gamma radiations for coarse grains as well as the contribution from alpha radiations in the case of fine grains. The contribution of cosmic radiation was taken into account and calculated according to Prescott and Hutton (1994). For coarse quartz grains an internal dose rate of 0.01 ± 0.002 Gy/ka was considered (Vandenberghé et al., 2008).

Sample code	Depth (cm)	U–Ra (Bq/kg)	Th (Bq/kg)	K (Bq/kg)	Meas. water content (%)	Grain size (µm)	De (Gy)	Total dose rate (Gy/ka)		Age (ka)		Relative random error calculated on age (%)			
								Measured water content	15% water	Measured water content	15% water	Measured water content	15% water		
STY-1.0	0.37	32.9 ± 1.4	30.9 ± 1.9	516 ± 19	12.7	4–11	quartz	17.0 ± 0.1 (n = 10)	3.25 ± 0.07	3.18 ± 0.07	5.2 ± 0.4	5.3 ± 0.5	2.4	2.4	
							pIRIR ₂₉₀	43 ± 1.1 (n = 10)	3.60 ± 0.08	3.52 ± 0.08	11.9 ± 1.0	12.2 ± 1.1	3.5	3.5	
							IR ₅₀	27.9 ± 1.3 (n = 10)	3.60 ± 0.08	3.52 ± 0.08	7.7 ± 0.7	7.9 ± 0.7	5.0	5.0	
STY-1.1	1.77	24.8 ± 3.8	30.7 ± 1.4	558 ± 19	2.8	63–90	quartz	12.1 ± 0.5 (n = 10)	2.79 ± 0.06	2.73 ± 0.06	4.4 ± 0.4	4.4 ± 0.4	5.0	4.9	
							4–11	quartz	56.0 ± 0.4 (n = 10)	3.48 ± 0.11	3.05 ± 0.09	16.1 ± 1.4	18.3 ± 1.6	3.1	3.1
							63–90	quartz	45.6 ± 1.5 (n = 10)	3.00 ± 0.09	2.65 ± 0.08	15.2 ± 1.1	17.2 ± 1.4	4.5	4.4
STY-2.1	2.30	28.0 ± 0.6	35.1 ± 1.0	574 ± 16	1.9	4–11	quartz	57.1 ± 0.5 (n = 10)	3.75 ± 0.06	3.26 ± 0.05	15.2 ± 1.3	17.5 ± 1.5	1.8	1.8	
							63–90	quartz	41.6 ± 1.0 (n = 10)	3.21 ± 0.05	2.8 ± 0.05	12.9 ± 0.8	14.8 ± 1.1	2.9	2.9
							4–11	quartz	56.2 ± 0.3 (n = 10)	3.96 ± 0.08	3.45 ± 0.07	14.2 ± 1.2	16.3 ± 1.3	2.0	2.0
STY-1.2	2.77	29.3 ± 1.2	34 ± 1.4	639 ± 18	2.2	4–11	pIRIR ₂₉₀	64.1 ± 2.1 (n = 10)	4.36 ± 0.08	3.79 ± 0.07	14.7 ± 1.3	16.9 ± 1.5	3.8	3.8	
							IR ₅₀	41.4 ± 1.1 (n = 10)	4.36 ± 0.08	3.79 ± 0.07	9.5 ± 0.8	10.9 ± 0.9	3.2	3.2	
							63–90	quartz	44.3 ± 1.7 (n = 10)	3.41 ± 0.07	2.98 ± 0.06	13.0 ± 0.9	14.9 ± 1.2	4.3	4.3
STY-2.2	3.30	31.0 ± 0.9	24.5 ± 0.6	551 ± 19	1.8	4–11	quartz	57.5 ± 0.5 (n = 10)	3.48 ± 0.07	3.02 ± 0.06	16.5 ± 1.4	19.0 ± 1.6	2.2	2.2	
							pIRIR ₂₉₀	70.6 ± 2.3 (n = 10)	3.84 ± 0.07	3.32 ± 0.06	18.4 ± 1.6	21.3 ± 1.8	3.8	3.8	
							IR ₅₀	37.9 ± 1.8 (n = 10)	3.84 ± 0.07	3.32 ± 0.06	9.9 ± 0.9	11.4 ± 1.1	5.0	5.0	
STY-1.3	3.79	33.2 ± 0.7	34.5 ± 1.6	578 ± 19	1.9	63–90	quartz	44.2 ± 1.0 (n = 10)	2.99 ± 0.06	2.61 ± 0.05	14.8 ± 0.9	16.9 ± 1.3	3.2	3.1	
							4–11	quartz	59.6 ± 0.5 (n = 10)	3.87 ± 0.08	3.35 ± 0.07	15.4 ± 1.4	17.8 ± 1.5	2.2	2.2
							63–90	quartz	46.8 ± 1.1 (n = 10)	3.29 ± 0.07	2.87 ± 0.06	14.2 ± 0.9	16.3 ± 1.2	3.1	3.1
STY-2.3	4.37	28.5 ± 0.8	22.5 ± 0.6	505 ± 17	2.9	4–11	quartz	59.6 ± 0.5 (n = 10)	3.15 ± 0.06	2.77 ± 0.05	18.9 ± 1.6	21.5 ± 1.8	2.2	2.2	
							63–90	quartz	47.9 ± 1.0 (n = 10)	2.71 ± 0.06	2.39 ± 0.05	17.7 ± 1.1	20.0 ± 1.5	3.0	3.0
							4–11	quartz	64.0 ± 0.6 (n = 10)	3.73 ± 0.09	3.51 ± 0.08	17.1 ± 1.5	18.2 ± 1.6	2.5	2.5
STY-1.4	4.87	35.8 ± 2.3	33.5 ± 1.8	620 ± 20	9.0	63–90	quartz	53.2 ± 1.6 (n = 10)	3.19 ± 0.07	3.0 ± 0.07	16.7 ± 1.2	17.7 ± 1.4	3.7	3.7	
							4–11	quartz	69.7 ± 0.8 (n = 12)	3.59 ± 0.09	3.25 ± 0.08	19.4 ± 1.7	21.5 ± 1.9	2.7	2.7
							pIRIR ₂₉₀	79.8 ± 2.7 (n = 10)	3.99 ± 0.1	3.59 ± 0.09	20.0 ± 1.8	22.2 ± 2.0	4.2	4.2	
STY-2.4	5.40	30.2 ± 2.8	35.4 ± 1.1	565 ± 19	5.4	4–11	IR ₅₀	55.0 ± 2.2 (n = 10)	3.99 ± 0.1	3.59 ± 0.09	13.8 ± 1.3	15.3 ± 1.4	4.7	4.7	
							quartz	59.7 ± 1.5 (n = 10)	3.06 ± 0.07	2.78 ± 0.07	19.5 ± 1.3	21.5 ± 1.7	3.5	3.5	
							quartz	70.5 ± 0.5 (n = 10)	3.64 ± 0.07	3.2 ± 0.06	19.4 ± 1.7	22.1 ± 1.9	2.1	2.1	
STY-1.5	5.87	34.1 ± 0.5	33.9 ± 1.2	530 ± 20	3.0	4–11	pIRIR ₂₉₀	88.5 ± 1.7 (n = 10)	4.06 ± 0.08	3.56 ± 0.07	21.8 ± 1.9	24.9 ± 2.2	2.7	2.7	
							IR ₅₀	52.4 ± 0.9 (n = 10)	4.06 ± 0.08	3.56 ± 0.07	12.9 ± 1.1	14.7 ± 1.3	2.6	2.6	
							63–90	quartz	57.6 ± 1.5 (n = 10)	3.08 ± 0.07	2.72 ± 0.06	18.7 ± 1.2	21.2 ± 1.6	3.4	3.4
STY-1.6	6.87	26.5 ± 0.3	28.7 ± 1.6	652 ± 21	10.5	4–11	quartz	81.7 ± 0.9 (n = 10)	3.42 ± 0.08	3.26 ± 0.07	23.9 ± 2.0	25.0 ± 2.1	2.5	2.5	
							pIRIR ₂₉₀	105 ± 2 (n = 10)	3.73 ± 0.08	3.56 ± 0.08	28.1 ± 2.3	29.5 ± 2.4	2.7	2.7	
							IR ₅₀	66.5 ± 2.4 (n = 10)	3.73 ± 0.08	3.56 ± 0.08	17.8 ± 1.6	18.7 ± 1.6	4.2	4.2	
STY-1.7	7.67	33.1 ± 0.1	35.6 ± 1.3	472 ± 17	2.2	63–90	quartz	77.1 ± 2.3 (n = 10)	2.97 ± 0.07	2.84 ± 0.06	26.0 ± 1.9	27.2 ± 2.2	3.8	3.8	
							4–11	quartz	121 ± 2 (n = 10)	3.47 ± 0.07	3.02 ± 0.06	34.9 ± 3.3	40.1 ± 3.7	2.7	2.7
							pIRIR ₂₉₀	180 ± 2 (n = 10)	3.90 ± 0.07	3.38 ± 0.06	46.1 ± 4.1	53.2 ± 4.6	2.0	2.0	
STY-1.8	8.70	47.0 ± 1.7	36.1 ± 1.8	497 ± 17	2.0	4–11	IR ₅₀	99.8 ± 1.8 (n = 10)	3.90 ± 0.07	3.38 ± 0.06	25.6 ± 2.3	29.5 ± 2.6	2.6	2.6	
							quartz	101 ± 5 (n = 10)	2.91 ± 0.06	2.55 ± 0.05	34.6 ± 2.7	39.6 ± 3.5	5.4	5.4	
							quartz	264 ± 2 (n = 10)	3.94 ± 0.08	3.42 ± 0.07	66.9 ± 6.4	77.2 ± 7.3	2.1	2.1	
STY-1.9	9.30	40.6 ± 0.7	38.8 ± 0.8	548 ± 19	2.2	63–90	pIRIR ₂₉₀	446 ± 8 (n = 10)	4.48 ± 0.09	3.87 ± 0.08	99.6 ± 9.2	115 ± 11	2.7	2.7	
							IR ₅₀	266 ± 8 (n = 10)	4.48 ± 0.09	3.87 ± 0.08	59.5 ± 5.7	68.9 ± 6.5	3.5	3.5	
							quartz	249 ± 12 (n = 11)	3.27 ± 0.07	2.85 ± 0.06	75.9 ± 5.7	87.2 ± 7.5	5.1	5.1	
STY-1.10	12.00	25.7 ± 0.6	24.3 ± 0.8	329 ± 15	2.3	4–11	quartz	301 ± 2 (n = 10)	4.00 ± 0.07	3.47 ± 0.06	75.3 ± 7.0	86.7 ± 7.9	1.9	1.9	
							pIRIR ₂₉₀	599 ± 21 (n = 10)	4.50 ± 0.07	3.89 ± 0.06	133 ± 13	154 ± 14	3.8	3.8	
							IR ₅₀	287 ± 10 (n = 10)	4.50 ± 0.07	3.89 ± 0.06	63.9 ± 6.0	73.8 ± 6.9	3.7	3.7	
STY-1.10	12.00	25.7 ± 0.6	24.3 ± 0.8	329 ± 15	2.3	63–90	quartz	215 ± 11 (n = 10)	3.33 ± 0.06	2.91 ± 0.05	64.3 ± 4.9	73.6 ± 6.5	5.3	5.3	
							4–11	quartz	556 ± 10 (n = 13)	2.47 ± 0.06	2.15 ± 0.05	225 ± 21	258 ± 24	2.9	2.9
							pIRIR ₂₉₀	–	–	–	–	–	–	–	
STY-1.10	12.00	25.7 ± 0.6	24.3 ± 0.8	329 ± 15	2.3	4–11	IR ₅₀	531 ± 33 (n = 8)	2.79 ± 0.06	2.42 ± 0.05	191 ± 21	220 ± 24	6.6	6.6	
							63–90	quartz	492 ± 30 (n = 11)	2.07 ± 0.05	1.81 ± 0.04	237 ± 20	271 ± 26	6.7	6.7

detectors as well as different moisture scenarios are presented in Supplementary File Table S3. Due to the highly comparable results, in the following only ages obtained through the ‘well detector’ data are being discussed and the dosimetric information used in age estimations is given in Table 1.

The dose rates were derived based on the conversion factors reported by Guérin et al. (2011). The measured water content estimation was based on the difference between the as sampled and the oven-dried (at 60 °C) weight of material from the inner part of the samples, with a relative error of 25%.

4. Results and discussion

4.1. Performance of the measurement protocols

For suitability of the SAR-OSL protocol for equivalent dose (D_e) estimation of these particular samples was tested in terms of recycling, IR depletion and recuperation tests. Rejection criteria for recycling ratio and IR depletion ratio tests were set as 10% deviation from unity. Recuperation values within 0.3% of the natural signal were exhibited by all the investigated aliquots, indicating that the growth curves pass very close to the origin and that thermal transfer during the SAR protocol is negligible. The equivalent doses were determined by projecting the sensitivity corrected natural OSL signal onto the dose response curve constructed in each case. The growth of the OSL signal was described by the sum of two saturating exponential functions. Examples of representative SAR growth curves for a single aliquot of fine (4–11 μm) and coarse (63–90 μm) grained quartz from samples of different ages (STY-1.2, 1.7 and 1.10; Fig. 1d–e) are given in Fig. 2. The OSL signals displayed a rapid decay during optical stimulation, the shape of the OSL decay curves for these samples being almost identical to that obtained for the calibration quartz supplied by the Risø National Laboratory. The insets discussed in Fig. 2 present typical OSL decay curves for aliquots of fine and coarse quartz grains from samples STY-1.2, STY-1.7 and STY-1.10, respectively.

A dose recovery test (Murray and Wintle, 2003) was employed to investigate the reliability of the equivalent doses obtained by applying the SAR protocol on fine and coarse quartz grains from samples STY-2.3 and STY-1.7. During this test, the natural aliquots were stimulated twice for 250 s at room temperature using the blue light emitting diodes. A 10 ks pause was inserted between the stimulations. The aliquots were then irradiated with known beta doses chosen to approximate the corresponding equivalent doses and measured using the SAR protocol (Murray and Wintle, 2000, 2003). A thermal treatment consisting of a 10 s preheat at 220 °C in combination with a test dose ramp heating to 180 °C (cutheat) was employed in the SAR protocol. A very good recovered to given dose ratio (with deviations from unity which do not exceed 10%) were obtained in all cases, indicating that the laboratory doses given prior to any heat treatment are measured with accuracy using the SAR protocol. The results are displayed in Supplementary File Table S4.

The variation in D_e as a function of preheat temperature was also investigated. Aliquots of fine and coarse quartz from samples STY-1.3 and STY-1.7 were separated in groups of four, each corresponding to a temperature point (180 °C, 200 °C, 220 °C, 240 °C, 260 °C, 280 °C); a cutheat temperature of 180 °C was used throughout the measurements. As shown in Supplementary File Fig. S2, the plateau observed validates the choice of a 220 °C preheat temperature.

Results of equivalent dose measurements and standard SAR performance tests are presented in Supplementary File Table S2. For each investigated sample, between 10 and 13 replicate measurements of the equivalent dose were performed. It is important

to note that none of the investigated aliquots in this study have been rejected due to, for example, poor recycling, IR depletion or recuperation values, which testifies for the good performance of the quartz extracted from all samples.

The equivalent doses of ten polymineral fine-grained (4–11 μm) samples (ie, STY-1.0, 1.2, 2.2, 2.4, 1.5, 1.6, 1.7, 1.8, 1.9 and STY-1.10) were measured by applying the post infrared stimulated luminescence (pIR-IRSL) using between eight and ten aliquots for each sample. A summary of the equivalent dose values (residuals subtracted) for pIR-IRSL₂₉₀ as well as for the values obtained using the preceding IR₅₀ measured signal is presented in Supplementary File Table S2. For residual dose estimation three aliquots of each sample were exposed to daylight for 22 days and then the residual doses were measured using the same parameters as in case of equivalent dose measurements. The values for the residual doses are shown in Supplementary File Table S5. The values obtained for samples from the Bug loess (Fig. 1d) are consistent with a mean residual dose value of 10 ± 2 Gy measured by Buylaert et al. (2011a) on polymineral fine-grains extracted from modern Chinese dust, while for the older samples values of 14 Gy (STY-1.8), 18 Gy (STY-1.9) and 25 Gy (STY-1.10) were obtained.

Representative dose response and decay curves for the pIR-IRSL₂₉₀ signals are also shown in Fig. 2 for three samples (STY-1.2, 1.7, 1.10). Recycling ratio, recuperation and dose recovery tests were applied. The recycling ratios are very close to unity for all samples (average values of 0.95 ± 0.01) and the recuperation values are also acceptable (<5%) (Supplementary File Table S2).

As the pIR-IRSL₂₉₀ protocol was originally designed for dating old samples the modified, less stringent temperature MET-pIRIR protocol suggested by Fu and Li (2013) was applied for STY-1.0 polymineral fine grains. The results are presented in Supplementary File Fig. S3 panel a). It can be seen that a plateau is not reached and the equivalent doses increase as function of stimulation temperature.

To test whether a given dose can be recovered using the pIR-IRSL protocol, a dose recovery test was applied to seven samples (STY-1.0, 2.4, 1.5, 1.6, 1.7, 1.8, 1.9). Three natural aliquots per sample were bleached under daylight. The aliquots were then given a beta dose similar to the measured D_e for that sample and the given dose measured. A satisfactory recovered to given dose ratio was obtained for samples with equivalent doses up to 200 Gy. For a given dose of 460 Gy (sample STY-1.8) an overestimation of 20% was observed, while in the case of a given dose of 616 Gy (sample STY-1.9) the overestimation is even more significant, amounting to 40%. The results are presented in Supplementary File Table S6. Previous studies on the pIR-IRSL signals of polymineral fine grains from the Danube loess stimulated at a high temperature (300 °C) resulted in obtaining overestimated values when conducting dose recovery tests for high given doses (~ 600 Gy), although satisfactory ratios were obtained for doses of 200 Gy or less (Vasiliniuc et al., 2012). This behaviour was attributed to potential dose dependent initial sensitivity changes. Here, for investigating the effect of stimulation temperature and further testing the accuracy of the pIR-IRSL₂₉₀ equivalent doses we applied the multi elevated temperature pIR-IRSL protocol (MET-pIRIR) (Li and Li, 2011) on polymineral fine grains (4–11 μm) of samples STY-2.4, STY-1.8, and STY-1.9 respectively. The results are presented in Supplementary File Fig. S3 (panels b, c and d). For STY-2.4 the equivalent doses obtained for stimulation temperatures in the 50 °C–150 °C range are increasing progressively, reaching a plateau for stimulation temperatures higher than 200 °C. This shows that the procedure is gradually discriminating fading and non-fading signals as found by Li and Li (2011). The equivalent doses obtained for this sample at high temperatures using the MET procedure are in excellent agreement with the equivalent dose obtained using the pIR-IRSL₂₉₀ protocol

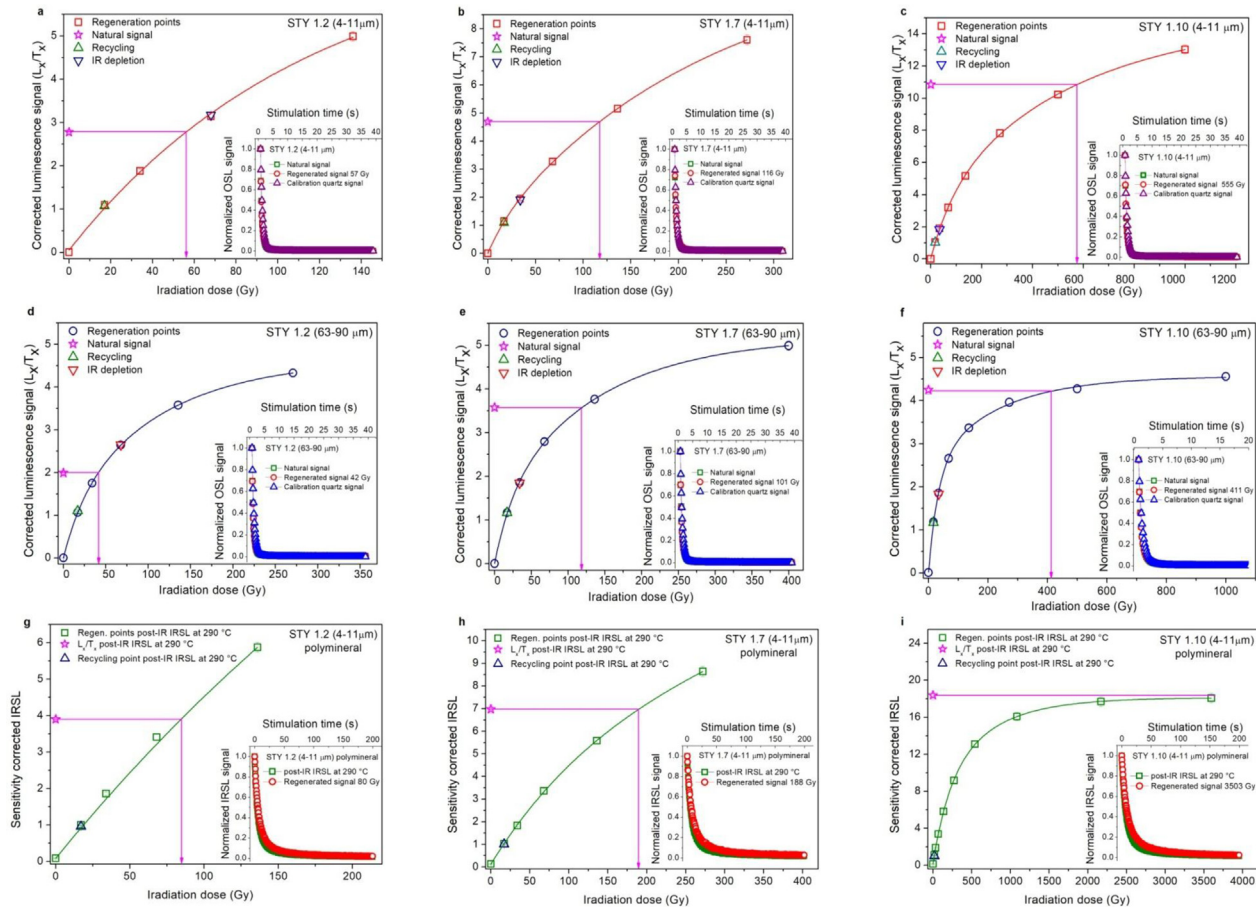


Fig. 2. Representative sensitivity-corrected dose response curves constructed for samples STY-1.2, STY-1.7 and STY-1.10 using one aliquot of (a), (b), (c) fine (4–11 μm) quartz grains, (d), (e), (f) coarse (63–90 μm) quartz grains and (g), (h), (i) polymineral fine grains, respectively. The response to regenerated doses is shown as open squares. The sensitivity corrected natural signal is depicted as a star and an arrow indicates the equivalent dose. Recycling and IR depletion points are represented as an open up triangle and an open inverted triangle, respectively. The inset shows a typical decay curve of natural CW-OSL signal (open squares) in comparison to a regenerated signal (open circles) and a calibration quartz signal (open triangles) in the case of quartz data, while for the post IR-IRSL₂₉₀ data natural signals are compared to regenerative signals.

(Supplementary File Table S2). This does not apply however for sample STY-1.8 for which the pIR-IRSL₂₉₀ equivalent dose of 460 Gy significantly overestimates the plateau MET-pIRIR equivalent dose of 355 Gy. For sample STY-1.9 a similar disagreement is reported between the pIR-IRSL₂₉₀ and MET-pIRIR equivalent doses. Also, in the case of sample STY-1.9 the MET-pIRIR equivalent dose obtained for a stimulation temperature of 250 °C does not seem to follow the plateau obtained in the 150–200 °C range.

4.2. Further investigations on the reliability of the equivalent doses obtained in the high dose range

For sample STY-1.10 collected from the Dnieper till (Fig. 1e) quartz OSL equivalent doses of ~500 Gy and ages older than 200 ka were obtained using (see Table 1 and Supplementary File Table S2). Such old ages derived via OSL dating methodology are seldom reported, while agreement between fine and coarse quartz OSL results in this age range is rather unprecedented (see Constantin et al., 2014; Timar-Gabor et al., 2017). For STY-1.10, natural pIR-IRSL₂₉₀ signals were found at laboratory saturation level.

We further examined the laboratory saturation characteristics of OSL and pIR-IRSL₂₉₀ signals by constructing extended SAR dose response curves for STY-1.10 using 3–4 aliquots. For fine (4–11 μm) quartz grains and polymineral fine grains laboratory doses up to 10000 Gy were given (Fig. 3a and b), whereas for coarse fraction

(63–90 μm) the maximum given dose was 5000 Gy (Fig. 3c). Additionally, the dose response curves of 180–250 μm quartz are presented (Fig. 3d), as we have previously shown that the saturation characteristics of quartz OSL are grain size-dependent (Timar-Gabor et al., 2017).

The growth of the signal with dose is best represented by the sum of two single saturating exponential functions such as in the following equation:

$$I(D) = I_0 + A(1 - \exp(-D/D_{01})) + B(1 - \exp(-D/D_{02})) \quad (1)$$

where, I is the intensity of the signal for a given dose D , I_0 is the intercept, A and B are the saturation intensities of the two exponential components and D_{01} , D_{02} are the dose levels characteristic of the dose–response curve of each exponential function (Wintle and Murray, 2006), parameters which we will refer to as saturation characteristics.

From data presented in Fig. 3 (along with detailed data obtained on individual aliquots presented in Supplementary File Fig. S4 and Table S7) it can be observed that the fine quartz fraction (4–11 μm) saturates at significantly higher doses than coarse (63–90 μm and 180–250 μm) fractions. In order rule out that the extended growth of the signal with dose in the case of fine quartz grains is attributed to feldspar contamination, three aliquots were bleached (as in a dose recovery test) and irradiated with a dose of 2000 Gy. The IR

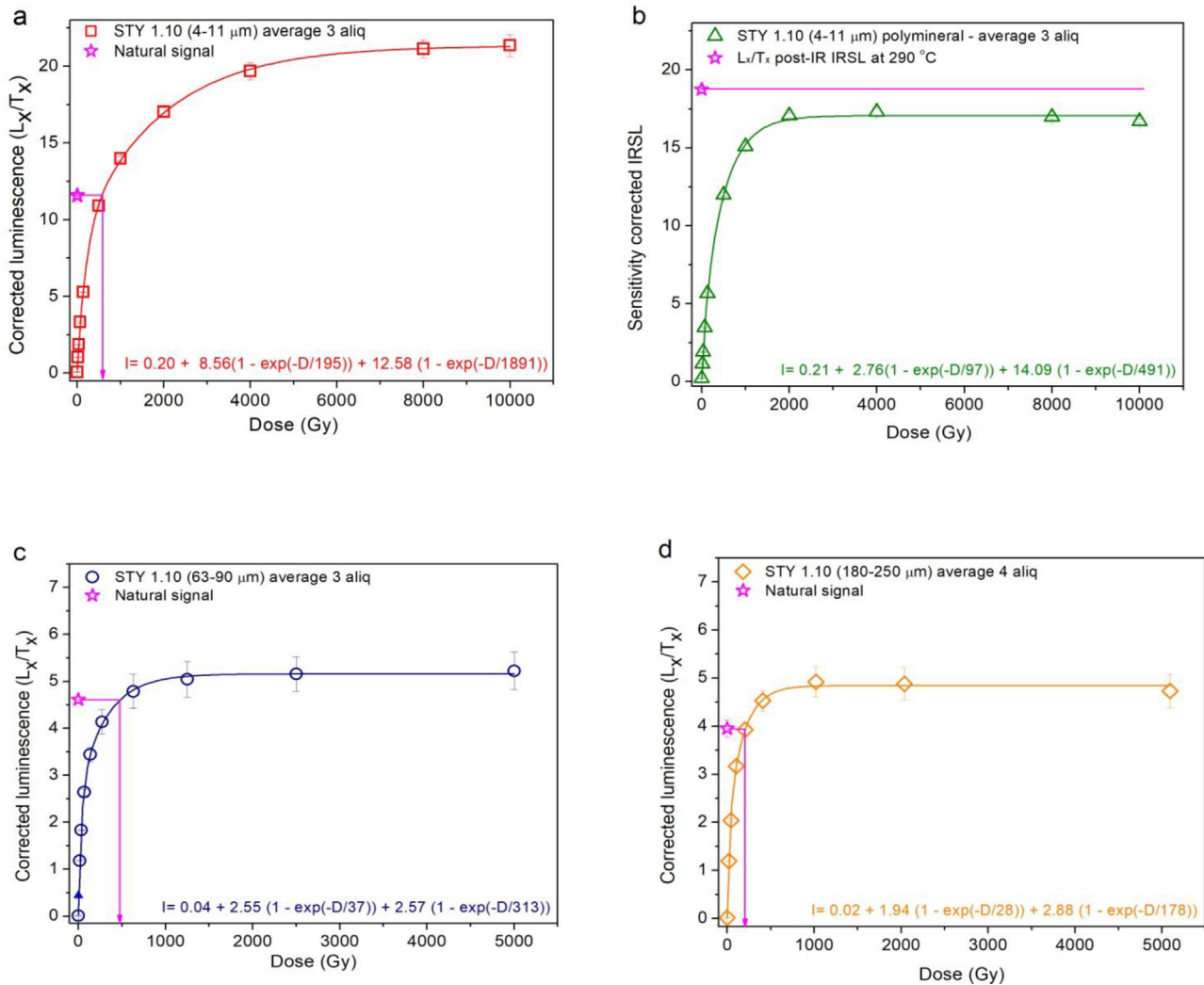


Fig. 3. Comparison between extended dose-response curves constructed for sample STY-1.10 using (a) fine 4–11 μm quartz grains, (b) 4–11 μm polymineral fine grains post IR-IRSL₂₉₀ signals, (c) coarse 63–90 μm and (d) 180–250 μm quartz grains. The growth patterns were best described by a sum of two saturating exponential functions. A test dose of 17 Gy was used throughout the measurements. Data presented is the average obtained on 3–4 aliquots.

signal was measured at 50 °C following a preheat of 220 °C. Another bleaching followed by an irradiation with 2000 Gy was subsequently performed and the OSL signal was measured at 125 °C. Both the IR and OSL signals were recorded using the Hoya UV 340 filter, as done during routine quartz OSL measurements. The intensity of the IR signal (integrated counts in 4 s of stimulation) was below 0.5% of the corresponding OSL signal intensity. Results of the experiment are presented in Supplementary File Fig. S5.

Similar results regarding the different saturation characteristics of fine and coarse quartz grains have been reported previously in loess samples from the Carpathian Basin, Lower Danube area, or the Chinese Loess Plateau (Timar-Gabor et al., 2012, 2015; 2017). For the 4–11 μm quartz fraction of sample STY-1.10 we are reporting average values for the saturation characteristics of $D_{01} = 195$ Gy and $D_{02} = 1891$ Gy, for the 63–90 μm fraction the corresponding values are $D_{01} = 37$ Gy and $D_{02} = 313$ Gy, whereas in the case of 180–250 μm fraction, saturation characteristics of $D_{01} = 28$ Gy and $D_{02} = 178$ Gy were determined. Consequently, the previously reported trend of grain size dependency of saturation characteristics (Timar-Gabor et al., 2017) also observed in the case of Quaternary terrestrial deposits in the Middle Dnieper area. Moreover, the saturation characteristics of fine quartz OSL signals seem to be

higher than the saturation characteristics of the pIR-IRSL₂₉₀ signal for which D_0 values of 97 Gy (D_{01}) and 491 Gy (D_{02}) are reported.

By comparing the normalised natural light levels to laboratory saturation light levels it can be noted that in case of both coarse quartz fractions (63–90 μm and 180–250 μm, respectively) the natural OSL signal is close to saturation, exceeding the 85% limit suggested by Wintle and Murray (2006) (Fig. 3c–d). Values indicative of the closeness to saturation of the natural signal for individual aliquots investigated are listed in Supplementary File Table S8 by presenting the ratio between the naturally corrected OSL and IRSL signals and the normalised light level corresponding to doses of 1000, 3595, 5000 or 10000 Gy. These doses were chosen based on the fact that they are high enough for the signal to reach saturation for the particular grain sizes and signals addressed.

It can be noted that the 85% limit suggested by Wintle and Murray (2006) is reached in the case of coarse quartz OSL, while for fine quartz natural OSL signals are found below saturation. Concerns raised by Wintle and Murray (2006) are referring mainly to the precision of measurement (when the signal is close to saturation) as in the region where the signal is above this limit, any uncertainty in the L_{nat}/T_{nat} will result in a larger and asymmetric uncertainty in the equivalent dose measured. However, recent

studies raised significant questions not only on the precision but also on the accuracy of the equivalent doses obtained in this dose range. Chapot et al. (2012) compared natural and laboratory dose response curves for quartz from Luochuan type section, Chinese Loess Plateau. A similar procedure was applied by Timar-Gabor and Wintle (2013) for the LPS at Costinesti, Romania. Both studies concluded that while the natural and the SAR laboratory dose response curves overlap at low doses, for doses higher than about 100–150 Gy there is no overlap, and thus the ages obtained should be treated with caution. It was suggested that this occurs because one of the main assumptions of luminescence dating is no longer fulfilled i.e., in the case of high doses, the natural growth of the signal cannot be reproduced by controlled irradiation in the laboratory. For Stayky samples reported here, the information available does not allow for constructing natural dose response curves.

Here, we have irradiated the 4–11 μm quartz fraction of sample STY-1.10 (natural sensitivity corrected signal denoted as L_n/T_n) with a beta dose of 3500 Gy on top of the natural dose that corresponds to an equivalent dose of 556 Gy, and further compared the luminescence response (denoted as L_n^*/T_n^*) to the response following a regenerative beta dose of 4000 Gy (denoted as L_x/T_x). A very small underestimation is reported (ratio of 0.96 ± 0.04), but within errors, the ratio is consistent to unity (Supplementary File Table S9). The same experiment was performed on the STY-1.10 63–90 μm quartz where a dose of 492 Gy was added on top of the natural accrued dose. The obtained ratio between L_n^*/T_n^* and L_x/T_x is consistent to unity (Supplementary File Table S9) showing that any improperly corrected dose dependent sensitivity change during the first measurement cycle is not relevant in the case of these samples. On the other hand, for fine quartz grains, the observed corrected signal increase with added dose from 11.1 ± 0.1 (L_n/T_n) to 17.7 ± 0.7 (L_n^*/T_n^*). This implies that if the signals of this sample were in field saturation, there is the possibility of some sort of dose dependent instability, either thermal or athermal affecting the signal, or a dose rate dependent sensitivity change in the case of high doses range affecting the laboratory dose response. Such investigations fall at the moment beyond the scope of the present study. However, due to the closeness to saturation of the signal in the case of coarse grains, and the concerns raised above in the case of fine grains the equivalent doses obtained on quartz for this sample should be regarded as minimum values and the corresponding ages as minimum ages.

As far as the pIR-IRSL₂₉₀ signals are concerned, the natural signal of STY-1.10 was found at the saturation level of the laboratory dose response curve (Fig. 3b). Thiel et al. (2011a), Thomsen et al. (2011), Buylaert et al. (2011a) and Murray et al. (2014) have observed signals consistent with saturation of the natural pIR-IRSL₂₉₀ signal on the laboratory growth curve from samples much older than the datable age range and interpreted this as evidence that the analysed signal does not suffer from anomalous fading.

4.3. Luminescence ages

The OSL ages obtained using two different grain sizes of quartz (4–11 μm and 63–90 μm respectively), along with the IR₅₀ and pIR-IRSL₂₉₀ ages calculated using different scenarios for the water content are presented in Table 1. Uncertainties of the ages were calculated following Aitken and Alldred (1972) and Aitken (1976). For a better visualisation in the stratigraphic context of Stayky section, these ages are also presented in Fig. 4, alongside the IRSL data reported by Rousseau et al. (2011).

From data in Figs. 4–5 it can be observed that all ages increase with depth; the pIR-IRSL₂₉₀ ages (Table 1) obtained for the Holocene sample (STY-1.0) overestimate the OSL ages on fine (5.3 ± 0.5 ka) or coarse (4.4 ± 0.4 ka) quartz. This is expected based on the

behaviour reported in the MET-pIRIR (Fu and Li, 2013) protocol (Supplementary File Fig. S3) and the comparison of these results to the pIR-IRSL₂₉₀ equivalent doses. It should be noted that similar overestimation of the pIR-IRSL₂₉₀ ages compared to quartz OSL ages has been observed when dating young (Holocene) sediments (Thiel et al., 2012; Giosan et al., 2018).

The pIR-IRSL₂₉₀ ages (~16.9–29.5 ka) obtained for sample STY-1.2 to STY-1.6 are in agreement within error limits with the OSL fine and coarse quartz ages (~16.3–25.0 ka) and give us confidence in the general reliability of our multi-methods results in this age range.

The OSL ages obtained on quartz for samples STY-1.8 and STY-1.9 (Table 1) are underestimating the pIR-IRSL₂₉₀ ages (Table 1; Fig. 4). It has been reported that quartz ages can underestimate the expected ages in high dose range (Murray et al., 2007; Buylaert et al., 2008; Lai, 2010; Timar et al., 2010; Lowick et al., 2010; Lowick and Preusser, 2011; Stevens et al., 2011; Timar-Gabor et al., 2011; Lai and Fan, 2013).

The applicability of the pIR-IRSL₂₉₀ protocol in dating old samples has been confirmed (Buylaert et al., 2012; Thiel et al., 2012) and previous evidence that pIR-IRSL₂₉₀ ages do not need fading correction (Thiel et al., 2011a; b; Thomsen et al., 2011; Murray et al., 2014) is further supported by the data presented in Fig. 2 showing that for sample STY-1.10, the pIR-IRSL₂₉₀ natural signal is not found below laboratory saturation level. As such, for these samples we consider that the pIR-IRSL chronology is more reliable than the quartz ages, although the overestimation observed for pIR-IRSL in the dose recovery test for doses higher than 400 Gy (section 4.1) requires further investigations. Based on these poor results in the dose recovery tests, as well as taking into account the overestimation reported by others when applying this protocol in the high dose range (Roberts, 2012; Vasiliniuc et al., 2012), we do not exclude at the moment the possibility that the pIR-IRSL equivalent doses obtained at least in the high dose range (>400 Gy) are overestimates. While further investigations are in progress on these matters, in general we consider the pIR-IRSL chronology more reliable than the quartz SAR-OSL ages in the case of samples STY-1.8 to STY-1.10.

The IR₅₀ ages obtained for all samples (Table 1, Fig. 4) appear underestimated. We attribute this to the fact that the infrared stimulated luminescence (IRSL) signal is hampered by anomalous fading (Wintle, 1973; Huntley and Lamothe, 2001). As such, the IR₅₀ ages will not be discussed further in data interpretation.

In Table 1 and Figs. 4–5 the luminescence ages are reported using both the 'measured' and an 'assumed' water content of 15% for all samples. The rationale behind this approach is twofold. First, while the 'measured' water content is usually considered in luminescence dating, a 15% water content was assumed previously for IRSL dating at Stayky (Rousseau et al., 2011). While past water content variations are hard to quantify, it is very likely that the moisture content was much higher in the past than the one found while sampling the exposed loess wall at N-Stayky. Second, as contradictory chronostratigraphic inferences have been made concerning the comparison of N-Stayky with other records (Rousseau et al., 2011; Kadereit and Wagner, 2014), the chronological data must be critically considered for unambiguous comparison of paleoclimate events.

4.4. Age-depth model

For visualisation of available data (Fig. 5) on an age-depth distribution (Supplementary File Figs. S6–S7), we apply the method discussed in Zeeden et al. (2018b), which constructs a probability density function for the random and systematic parts of uncertainty and uses only the random part for reducing uncertainty (see

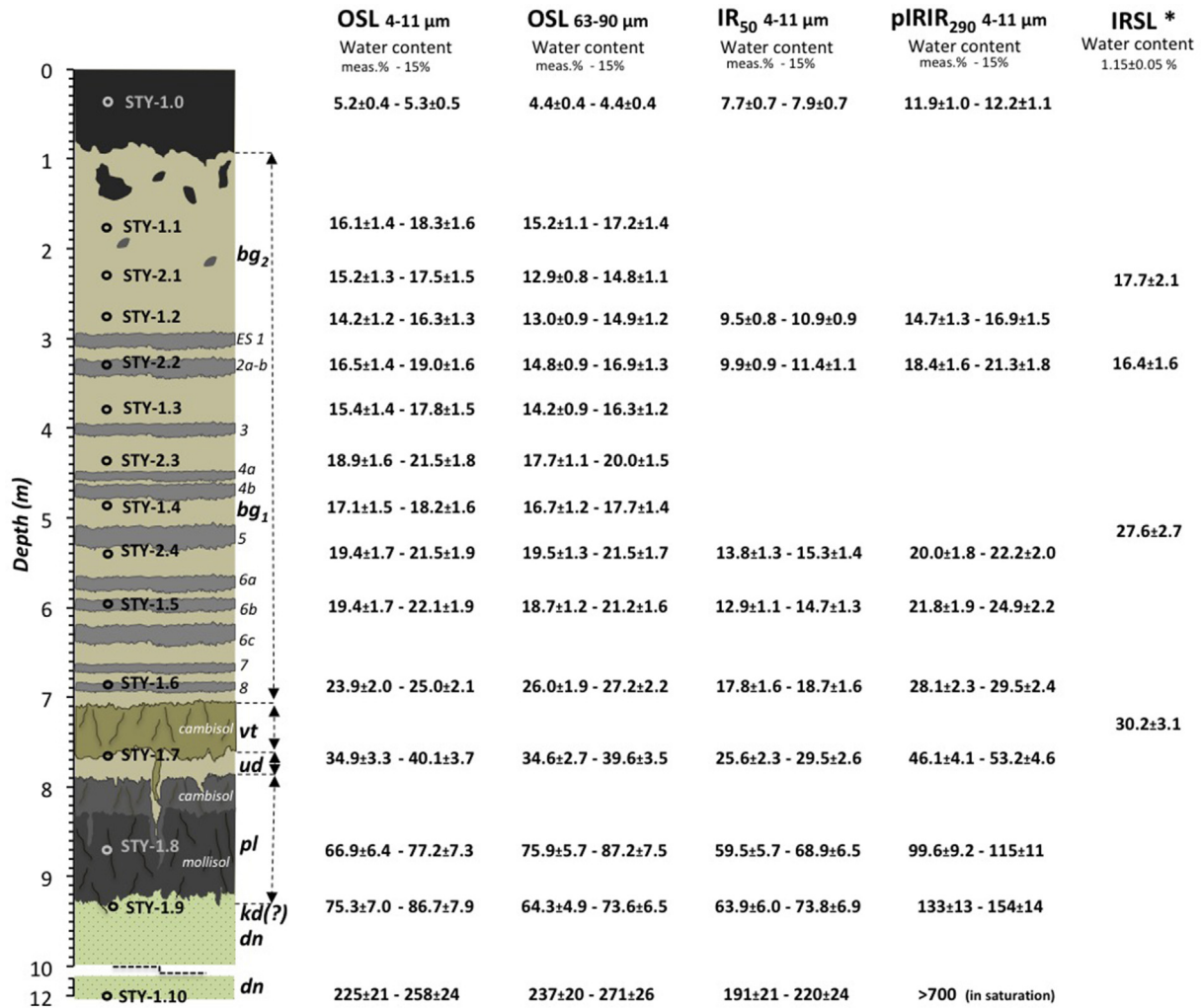


Fig. 4. Schematic representation of the lithostratigraphy of N-Stayky profile following Rousseau et al. (2011) and our observations, and the depth distribution of multi-method luminescence dating results (in ka) discussed in this study. * IRSL data from Rousseau et al. (2011).

last columns of Table 1). This is in our opinion a robust method for treating luminescence data, with more realistic results than interpolation of data by linear or polynomial fits (De Vleeschouwer and Parnell, 2014). Bayesian age–depth modelling of luminescence data (ie., Blaauw et al., 2010; Stevens et al., 2011) can only reduce uncertainty of the random uncertainty, and not of systematic bias (Zeeden et al., 2018b). The age–depth models shown in Supplementary File Figs. S6–S7 were established for visualising the likely chronological range of the embryonic soils within the Bug loess (Figs. 4–5). We thus limited the application of age–depth modelling to samples STY-1.0 to STY-1.6 from Bug loess (and STY-1.7 from Vytachiv paleosol), as there is increased confidence in the accuracy of these ages following the agreement between results obtained using the different luminescence methods applied (Supplementary File Figs. S6–S7).

5. Paleoenvironmental and chronostratigraphic implications

5.1. Dating the Dnieper till, Pryluky pedocomplex and Vytachiv paleosol

As discussed previously, due to the saturation of luminescence signals, providing a reliable age for sample STY-1.10 from the

Dnieper till was not possible despite the application of multiple luminescence dating techniques. Furthermore, for pIR-IRSL₂₉₀, the natural signals were found in saturation and thus the minimum equivalent dose should be ~2000 Gy, corresponding to an age of about 700 ka. Considering the complex stratigraphy of the Dnieper unit (Veklitch, 1993; Rousseau et al., 2001, 2011; Gerasimenko, 2006; Kunitsa, 2007; Lindner et al., 2006; Matviishina et al., 2010; Gozhik et al., 2014), for more reliable chronological insights, further research must be carried out on the emplacement ages and paleoenvironmental significance of each bed within this unit.

Sample STY-1.9 collected from the Cca horizon of Pryluky mollisol overprinting the underlying loams was OSL dated to 75.3 ± 7 ka - 86.7 ± 7.9 ka on fine quartz and 64.3 ± 4.9 ka - 73.6 ± 7.5 ka on coarse quartz (Fig. 4). The pIR-IRSL₂₉₀ dating provided much older ages in the range of 133 ± 13 ka to 154 ± 14 ka, respectively. Sample STY-1.8 collected from the top half of A1 horizon of Pryluky mollisol was dated to 66.9 ± 7.4 ka - 77.2 ± 7.3 ka (4–11 μm) and 75.9 ± 5.7 ka - 87.2 ± 7.5 ka (63–90 μm) (Fig. 4). The pIR-IRSL₂₉₀ dating provided ages of 99.6 ± 9.2 ka to 115 ± 11 ka. As discussed above, quartz ages based on equivalent doses in this range should be regarded as minimum ages and we consider the pIR-IRSL₂₉₀ data (Table 1; Fig. 4) to be more reliable for these samples. Albeit our dating

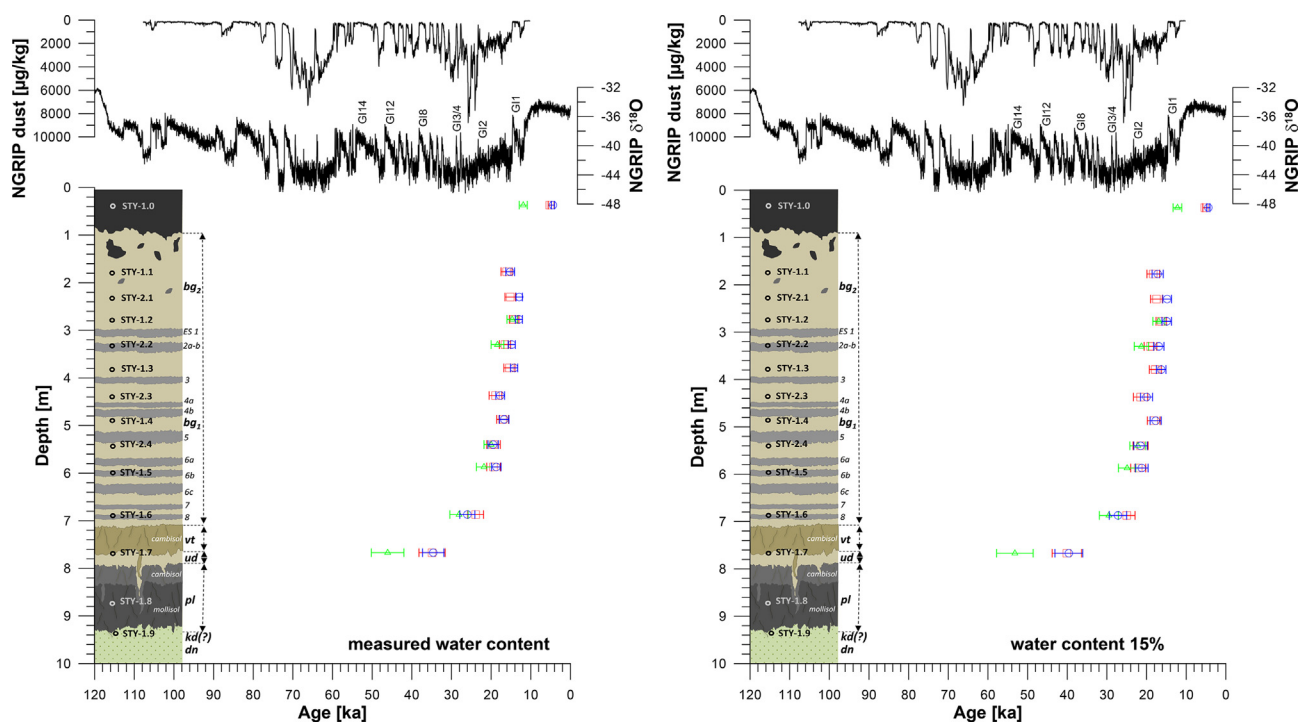


Fig. 5. Schematic representation of the lithostratigraphy of N-Stayky profile (Rousseau et al., 2011), and the depth distribution of luminescence data (at 1σ) for samples STY-1.0 to STY-1.7 in a comparison with NGRIP $\delta^{18}\text{O}$ data and mineral dust data on the GICC05 timescale (Ruth et al., 2007; Svensson et al., 2008). Ages based on 'measured water content' (left panel) and an 'assumed 15% water content' (right panel) for OSL fine grain (4–11 μm) quartz in red squares, OSL coarse grain (60–93 μm) quartz in blue circles, and post-IR IRSL₂₉₀ polymineral grains in green triangles. (For interpretation of the references to colour in this figure legend, the reader is referred to the Web version of this article.)

resolution is limited for attempting the identification of MIS 5 paleoclimate events supposedly represented by the Pryluky pedocomplex (cf., Rousseau et al., 2011; Kadereit and Wagner, 2014), the pIR-IRSL₂₉₀ data indicate MIS 5 ages for the mollisol (Fig. 4). Considering that Pryluky unit comprises also another paleosol (ie, the cambisol), it is thus likely that at N-Stayky this unit corresponds broadly to MIS 5. Whereas only two paleosols are found at N-Stayky, and these impacted by cryogenic and possibly erosional processes, in other sections the Pryluky pedocomplex preserves three to five distinct horizons (Veklich, 1993; Nawrocki et al., 1999; Rousseau et al., 2001; Gerasimenko, 2006; Gozhik et al., 2014; Haesaerts et al., 2016). Moreover, a grey-ochre hydromorphic soil with vertical root channels and weak prismatic structure overlain by the Pryluky pedocomplex has been described in Stayky area (Karmazinenko, 2010; Rousseau et al., 2011). Rousseau et al. (2011) suggested this soil formed during the Eemian (i.e., MIS 5e) and linked it tentatively to the Kaydaky unit. In this case, the Pryluky pedocomplex would be younger than MIS 5e. This hydromorphic soil is preserved only in places, but at S-Stayky, in the same stratigraphic position, a grey forest paleosol has been noted, also related to the Kaydaky unit by Veklich (1968). These short-scale pedostratigraphic discrepancies further illustrate the complexity of MIS 5/MIS 6 environmental response in the Middle Dnieper area, calling for further radiometric dating to achieve a thorough evaluation of regional MIS 5 correlations.

The Vytachiv (vt) pedocomplex in stratigraphically complete sections in the Middle Dnieper area consists of three paleosols (Gerasimenko, 2006; Bokhorst et al., 2011; Gozhik et al., 2014), each in turn overlain by an embryonic soil. This points to several distinct phases of pedogenesis. It is very likely that Vytachiv cambisol at N-Stayky preserving a very distinctive Cca horizon (Rousseau et al., 2011) relates only to the middle paleosol of the tripartite Vytachiv pedocomplex elsewhere (Gerasimenko, 2006; Bokhorst et al.,

2011; Gozhik et al., 2014). Further, Rousseau et al. (2011) IRSL dated the middle part of Vytachiv cambisol to 30.2 ± 3.1 ka (Fig. 4), whereas sample STY-1.7 collected from the Cca horizon close to the transition to the underlying Uday loess provided OSL ages of 34.9 ± 3.3 ka - 40.1 ± 3.7 ka (4–11 μm) to 34.6 ± 2.7 ka - 39.6 ± 3.5 ka (63–90 μm). The pIR-IRSL₂₉₀ dating returned ages between 46.1 ± 4.1 ka and 53.2 ± 4.6 ka. Sample STY-1.6 from the overlying ES 8 (within Bug loess) provided ages of 23.9 ± 2 ka and 25 ± 2.1 ka for fine quartz, 26.0 ± 1.9 ka and 27.2 ± 2.2 ka for coarse quartz, and respectively 28.1 ± 2.3 ka and 29.5 ± 2.4 ka for pIR-IRSL₂₉₀ dating (Figs. 4–5).

Albeit the good agreement between the dated quartz grain sizes and the pIR-IRSL₂₉₀ results for STY-1.6 (Table 1), there is a noticeable difference for STY-1.7, with OSL data indicating middle-to-late MIS 3 ages and pIR-IRSL₂₉₀ data early-to-middle MIS 3 age ranges instead (Figs. 4–5). Based on luminescence investigations in this age range and results from intrinsic rigour behaviour tests, one cannot assess with certainty whether quartz OSL or feldspars pIR-IRSL₂₉₀ data are more accurate. Kadereit and Wagner (2014) argued that the Vytachiv paleosol at N-Stayky is likely an equivalent of GI-7 or even GI-5, but possibly even younger, whereas Rousseau et al. (2011) proposed that it started forming synchronously with GI-8. Based on our results, it is possible that it either represents a stack of interstadials within MIS 3 rather than just one GI event, or it has been affected by erosional truncation. Indeed, cryogenic features strongly impacted this paleosol at N-Stayky (Rousseau et al., 2011) as well as the underlying Uday (presumably MIS 4) loess (Rousseau et al., 2001; Lindner et al., 2006). Furthermore, the age range of STY-1.6 indicates that ES8 formed at the onset of the Late Pleniglacial, at or after the MIS 3/2 transition (Fig. 4). As the underlying thin loess bed exhibits a sharp and undulating lower boundary (Rousseau et al., 2011), an erosional discontinuity between the Vytachiv paleosol and the overlying Bug loess is also a possibility.

Pollen data for Vytachiv unit document the predominance of pine forests, with an admixture of spruce and broad-leaved trees (Veklich et al., 1984; Gerasimenko, 2006). Similar vegetation composition coupled with intervals of higher organic productivity denoting interstadial conditions has been documented at similar latitudes in Europe for early-to-middle MIS 3 (Caspers and Freund, 2001; Wohlfarth et al., 2008; Fletcher et al., 2010; Sirocko et al., 2016). It is thus plausible that the tripartite Vytachiv unit elsewhere (Gerasimenko, 2006, 2010; Bokhorst et al., 2011) might also comprise a series of GI events within MIS 3, rather than strictly just one interstadial per paleosol. Support for this assertion is provided by the Maksymivka sequence, where Vytachiv unit comprises four distinctly differentiated horizons. The radiometric data discussed in Gozhik et al. (2014) suggest that at Maksymivka this unit likely comprises most of MIS 3.

Thus, relating the Vytachiv unit at N-Stayky with the Greenland event stratigraphy as discussed in Rousseau et al. (2011, 2017b) and Kadereit and Wagner (2014) is challenging in the light of existing chronological data and stratigraphic evidence. Increased dating resolution appears necessary before correlations on event-to-event basis may be unambiguously validated (cf. Vandenberghe and van der Plicht, 2016). This is even more compelling, as the Vytachiv paleosol is considered the equivalent of Lohner Boden (LB) in central-western Europe (Antoine et al., 2001; Rousseau et al., 2011; Gocke et al., 2014; Moine et al., 2017). However, as the chronometric results of Moine et al. (2017) point to a broad temporal range for the pedogenetic phase represented by the LB, its value (and of other pedological horizons in that age range) as a chronostratigraphic marker should also be regarded with caution (Kadereit et al., 2013; Terhorst et al., 2014; Lehmkuhl et al., 2016; Sauer et al., 2016; Rousseau et al., 2017b; Lisá et al., 2018).

5.2. The Bug (bg) loess and the pervasive MIS 2 embryonic soils

The age range for sample STY-1.6 collected from ES8 (Figs. 4–5) has been discussed previously. Sample STY-1.5 from the middle soil bed within ES6 (Figs. 1d and 4) provided OSL fine quartz ages of 19.4 ± 1.7 ka and 22.1 ± 1.9 ka, and 18.7 ± 1.2 ka to 21.2 ± 1.6 ka for coarse quartz. There is an excellent agreement between OSL data and the pIR-IRSL₂₉₀ results in the range of 21.8 ± 1.9 ka and 24.9 ± 2.2 ka.

ES5 is the most developed among all embryonic soils (Fig. 1d), being traceable in other sections where usually only one such embryonic soil (i.e., likely ES5) is described within the Bug loess (Chlebovsky et al., 2003; Gozhik et al., 2014). The differentiation of ES5 into genetic horizons indicates stronger pedogenesis compared to the other embryonic soils (Gerasimenko, 2006; Rousseau et al., 2011). Sample STY-2.4 collected from ES5 has been dated to 19.4 ± 1.7 ka and 21.5 ± 1.9 ka on fine quartz, and 19.5 ± 1.3 ka to 21.5 ± 1.7 ka on coarse quartz. The pIR-IRSL₂₉₀ ages of 20.0 ± 1.8 ka and 22.2 ± 2.0 ka are highly comparable with the OSL data (Table 1). Given these results, as well as these for STY-1.6 (Fig. 4), it is tempting to compare ES5–ES6 with the soil horizons dated to around 21 kyr BP in several loess records from central-western Europe (Dambon et al., 1996; Fuchs et al., 2013; Meszner et al., 2013; Terhorst et al., 2014; Moine et al., 2017). However, the ages reported here are younger compared to the 27.6 ± 2.7 ka IRSL age previously reported by Rousseau et al. (2011) for the same pedogenetic horizon at N-Stayky (Fig. 4).

The dating of seven more samples from STY-1.4 to STY-1.1 (Figs. 1d and 4) comprising six ES horizons (from ES4 to ES1) and the interbedded loess (including sub-unit bg₂) provided very comparable OSL ages in the range of ~19–14 ka or ~21–13 ka depending on the water content used (Table 1). The pIR-IRSL₂₉₀ ages obtained for several pilot samples further support the OSL

results (Figs. 4–5). The data demonstrate the high accumulation rates during this time interval, similar to evidence from other loess sites in eastern Europe (Fitzsimmons and Hambach, 2014; Obrecht et al., 2017; Zeeden et al., 2018). The N-Stayky section is capped by the Holocene mollisol, a typical chernozem, with the OSL ages of ~4.0–5.3 ka (STY-1.0) linking the emplacement time of its A1 horizon to mid-Holocene, when an intensification of humus accumulation was observed in the forest-steppe and steppe soils of eastern Europe (Ivanov and Chendev, 2015).

The paleoclimate significance of the embryonic soils in the N-Stayky bg₁ loess is intriguing. Fig. 5 shows the luminescence data discussed here, alongside comparison with NGRIP $\delta^{18}\text{O}$ and mineral dust content (Ruth et al., 2007; Svensson et al., 2008; Rasmussen et al., 2014). These proxies, for temperature and dust cycling in the high latitudes respectively are often discussed in connection with regional expression of rapid climate variability in the North Atlantic region and beyond (Rousseau et al., 2001, 2011, 2017a; b; Svensson et al., 2008; Wohlfarth et al., 2008; Fleitmann et al., 2009; Veres et al., 2009, 2013a; Blaauw et al., 2010; Fletcher et al., 2010; Moreno et al., 2010; Shumilovskikh et al., 2014; Luetscher et al., 2015; Sirocko et al., 2016; Moine et al., 2017).

As it can be visualized in Fig. 5, all embryonic pedogenetic horizons starting with ES8 would be younger than GI-4, or even GI-3, as chronologically defined in the Greenland ice data (Rasmussen et al., 2014). This is irrespective of the water content used in defining age ranges (Fig. 4), or the luminescence method employed (Table 1; Supplementary File Figs. S6–S7). As such, the dating of the Bug loess raises implications concerning both the chronological span of these embryonic soils and the forcing mechanisms that controlled their development. First, the embryonic soils, several of them clearly well developed, would indicate favourable hydroclimate conditions for vegetation development (Gerasimenko, 2006) and pedogenesis (see discussion in Rousseau et al., 2011, 2017a; Kadereit and Wagner, 2014; Moine et al., 2017 on thresholds for soil formation in periglacial environments during the last glacial). Higher percentages of organic carbon in the embryonic soils compared to the embedding loess support this hypothesis (Rousseau et al., 2011). Additionally, mollusk assemblages (Kunitsa, 2007) support pollen data (Gerasimenko and Rousseau, 2008), indicating wetter paleoenvironments for the embryonic soils as compared to the embedding loess.

Secondly, based on the chronostratigraphic range defined here (Figs. 4–5), most of the ES formed in the interval 29/27–15 kyr BP, but mainly immediately after 20 kyr BP. With exception of GI-2 (Fig. 4), no interstadial events are documented in Greenland ice isotopic (Svensson et al., 2008; Rasmussen et al., 2014) or greenhouse gas data (Fischer et al., 2008; Baumgartner et al., 2014) for the interval postdating GI-3 and up to GI-1. Nevertheless, a steady increase denoting an early warming is observed in Greenland data from about 20 kyr BP (Kindler et al., 2014). Ameliorating environmental conditions post last glacial maximum are also documented in pollen (Caspers and Freund, 2001; Fletcher et al., 2010; Magyari et al., 2014; Sirocko et al., 2016) or speleothem data (Moreno et al., 2010; Luetscher et al., 2015). Furthermore, interesting analogues can be drawn with evidence of regional paleohydrological variability during the last deglaciation. For example, for the interval 20–15 kyr BP, several red clay layers were deposited in the Black Sea, each depositional phase lasting around 200 years (Bahr et al., 2006; Ménot and Bard, 2012; Rostek and Bard, 2013). They were interpreted as terrigenous input by the major rivers including Dniester draining into the Black Sea. Organic geochemical proxies, including terrestrial biomarkers (Bahr et al., 2006; Ménot and Bard, 2012; Rostek and Bard, 2013) indicate run-off increase and erosion, denoting perhaps short-term regional hydroclimate variability that might parallel the timing of some of the embryonic soils seen at N-

Stayky, or elsewhere in central-western Europe (Antoine et al., 2001, 2013; Kusiak et al., 2012; Fuchs et al., 2013; Meszner et al., 2013; Gocke et al., 2014; Rousseau et al., 2011, 2017b). Speleothem data from eastern Mediterranean cave records (Fleitmann et al., 2009; Badertscher et al., 2011 and references therein) also indicate prominent hydrological changes in the interval 20–15 kyr BP. Moreover, similar developments have been documented for the Atlantic margin, with increased input of terrestrial organic matter into the ocean linked to hydrological changes on land (Ménot et al., 2006; Toucanne et al., 2015). It is not yet clear whether these events were linked to rainfall patterns that allowed for short phases of pedogenesis over large areas, or that they represent rather local phenomena linked to reactivation of the fluvial systems following melt-water pulses from the European ice-sheets (Ménot et al., 2006). Toucanne et al. (2015) suggested that the waxing and waning of Late Pleistocene ice sheets following the Northern Hemisphere summer insolation increase from about 23 kyr BP induced shifts in the North Atlantic storm track patterns (and thus in rainfall variability), presumably in a similar manner as reconstructed by Naafs et al. (2013) or Luetscher et al. (2015).

Nevertheless, in Nussloch LPS (Antoine et al., 2001; Moine et al., 2017) a chronologically much better resolved record to which N-Stayky has been compared (Rousseau et al., 2011, 2017a; b), several embryonic (tundra-gley) soils developed between the equivalent of GI-3 and the Holocene topsoil. Except for GI-2, these embryonic soils could not be linked to the Greenland isotope stratigraphy following a close comparison of late MIS 3–2 paleoclimate events, as achieved between Nussloch and the ice core data (Moine et al., 2017; Rousseau et al., 2017a; b). As such, these enigmatic pedogenetic phases would indicate that terrestrial environments in the European mid-latitude loess fields experienced significantly more hydroclimate variability than previously considered for MIS 2. It remains to be established whether such short-term, but regionally well-expressed pedogenetic phases (Haesaerts et al., 2010, 2016; Rousseau et al., 2011, 2017a; Moine et al., 2017) are representative in the broader hydroclimate system (Bahr et al., 2006; Ménot et al., 2006; Bokhorst et al., 2011; Ménot and Bard, 2012; Naafs et al., 2013; Rostek and Bard, 2013; Sima et al., 2013; Luetscher et al., 2015; Toucanne et al., 2015), or that they represent mainly regional/local phenomena with insufficient chronological control within and/or between different records (Kadereit et al., 2013; Kadereit and Wagner, 2014; Lehmkuhl et al., 2016; Sauer et al., 2016).

6. Conclusions

Detailed OSL investigations were performed on quartz of different grain sizes and ages collected from the loess-paleosol sequence at N-Stayky, Ukraine. For samples encompassing the Bug loess unit, ages ranging from ~15 ka to ~27/29 ka have been obtained, the investigated quartz grain size fractions (4–11 μm and 63–90 μm) being in perfect agreement. Such an agreement in this age range has previously been reported for loess (Timar-Gabor et al., 2017), and further confirmed by comparison with independent age control provided through tephrochronology (Constantin et al., 2012; Veres et al., 2013b; Anechitei-Deacu et al., 2014) or radiocarbon dating (Trandafir et al., 2015). Therefore, we are confident in the methodological and chronological accuracy of the OSL ages that constrain the depositional time of Bug unit at N-Stayky to MIS 2. Confidence in the accuracy of these results was increased through pIR-IRSL₂₉₀ dating that supports the OSL chronology for the Bug unit. Deriving a reliable multi-method chronological framework for the Bug loess is critical in the light of previous discussions on the paleoclimate correspondence between a series of embryonic soils and Greenland interstadial rapid climate

variability and our multi-method luminescence data demonstrate that these short-term phases of soil formation took place during MIS 2, between ~27 and 29 to 15 ka. As no corresponding variability is seen in ice core isotope data, the results point to complex hydroclimate variability during the last deglaciation over the mid-latitudes loess fields of Europe that require further investigations.

The dating of samples roughly bracketing the Vytachiv paleosol, previously debatably linked to various interstadial events within MIS 3 indicate that it developed during middle-to-late MIS 3. It is thus likely that this part of the Stayky record is either not continuous, or that it encompasses a broader age range within MIS 3 than previously considered; this would not allow for an unambiguous linking of this paleosol with specific GI event(s) as previously suggested.

For samples collected from the transition and respectively into the Pryluky unit, as well as in the underlying Dnieper unit, ages of ~70, ~80 and ~250 ka were obtained using quartz OSL. Application of feldspar dating on polymineral fine grains for the same samples from the Pryluky unit indicate that the OSL results should be regarded as minimum, as ages of 90 ka to 126 ka (in mollisol) and 120 ka to 168 ka (in underlying loams) considering the error limits and different water contents were obtained by the application of pIR-IRSL₂₉₀ protocol. These results confirm that this pedocomplex at Stayky likely has been emplaced during MIS 5.

For the sample collected from the Dnieper till, in the case of coarse quartz grains (63–90 μm as well as 180–250 μm) the natural OSL signals were close to saturation (~85% of maximum light level or higher). Polymineral fine grains pIR-IRSL₂₉₀ signals from the same sample were found to be in saturation. On the contrary, in the case of 4–11 μm quartz, the natural OSL signals were at about 50–60% from the maximum laboratory light levels. These results further caution on the application of quartz OSL dating for old samples, especially by employing the fine quartz fraction. Establishing the exact limit of quartz OSL dating applicability requires further research. It is important to note however that the corresponding equivalent doses for the samples on which agreement between fine quartz, coarse quartz and pIR-IRSL₂₉₀ is reported here are lower than the 100–150 Gy limit of accurate quartz OSL dating (Chapot et al., 2012; Timar-Gabor and Wintle, 2013). This is based on the comparison of natural and laboratory generated dose response curves on Chinese and Romanian loess, as well as the limit suggested by Timar-Gabor et al. (2017) based on the comparison of dose response curves of different grain sizes of quartz from various locations around the world. Overall, the multi-method luminescence dating of Stayky clarified several previously un-resolved chronostratigraphic issues, suggesting that at least for MIS 2, this record could be considered as a reference site in mid-latitude European loess paleoclimatology.

Acknowledgements

This project has received funding from the European Research Council (ERC) under the European Union's Horizon 2020 research and innovation programme ERC-2015-STG (grant agreement No [678106]). The authors are grateful to A. Vulpoi, S. Kelemen and V. Anechitei-Deacu for help with SEM analysis, gamma spectrometric measurements and sample preparation and to J. Longman for English language proofreading. Comments and suggestions by an anonymous reviewer and J. Vandenberghe greatly improved the manuscript.

Appendix A. Supplementary data

Supplementary data to this article can be found online at <https://doi.org/10.1016/j.quascirev.2018.09.037>.

References

- Aitken, M.J., 1976. Thermoluminescence age evaluation and assessment of error limits: revised system. *Archaeometry* 18, 233–238.
- Aitken, M.J., Allred, J.C., 1972. The assessment of error limits in thermoluminescence dating. *Archaeometry* 14, 257–267.
- Ampel, L., Wohlfarth, B., Risberg, J., Veres, D., 2008. Paleolimnological response to millennial and centennial scale climate variability during MIS 3 and 2 as suggested by the diatom record in Les Echets, France. *Quat. Sci. Rev.* 27, 1493–1504. <https://doi.org/10.1016/j.quascirev.2008.04.014>.
- Anechitei-Deacu, V., Timar-Gabor, A., Fitzsimmons, K.E., Veres, D., Hambach, U., 2014. Multi-method luminescence investigations on quartz grains of different sizes extracted from a loess section in southeast Romania interbedding the Campanian Ignimbrite ash layer. *Geochronometria* 41, 1–14. <https://doi.org/10.2478/s13386-013-0143-4>.
- Antoine, P., Rousseau, D.D., Zöller, L., Lang, A., Munaut, A.V., Hatté, C., Fontugne, M., 2001. High resolution record of the last interglacial–glacial cycle in the Nussloch loess–paleosol sequences, upper Rhine area Germany. *Quat. Int.* 76–77, 211–229. [https://doi.org/10.1016/S1040-6182\(00\)00104-X](https://doi.org/10.1016/S1040-6182(00)00104-X).
- Antoine, P., Rousseau, D.D., Degeai, J.P., Moine, O., Lagroix, F., Kreutzer, S., Fuchs, M., Hatté, C., Gauthier, C., Svoboda, J., Lisa, L., 2013. High-resolution record of the environmental response to climatic variations during the Last Interglacial–Glacial cycle in Central Europe: the loess–paleosol sequence of Dolní Věstonice (Czech Republic). *Quat. Sci. Rev.* 67, 17–38. <https://doi.org/10.1016/j.quascirev.2013.01.014>.
- Bábeek, O., Chlachula, J., Grygar, T.M., 2011. Non-magnetic indicators of pedogenesis related to loess magnetic enhancement and depletion: examples from the Czech Republic and southern Siberia. *Quat. Sci. Rev.* 30, 967–979. <https://doi.org/10.1016/j.quascirev.2011.01.009>.
- Badertscher, S., Fleitmann, D., Cheng, H., Edwards, R.L., Göktürk, O.M., Zümbühl, A., Leuenberger, M., Tüysüz, O., 2011. Pleistocene water intrusions from the Mediterranean and Caspian seas into the Black Sea. *Nat. Geosci.* 4, 236–239. <https://doi.org/10.1038/ngeo1106>.
- Bahr, A., Arz, H.W., Lamy, F., Wefer, G., 2006. Late glacial to Holocene paleoenvironmental evolution of the Black Sea, reconstructed with stable oxygen isotope records obtained on ostracod shells. *Earth Planet. Sci. Lett.* 241, 863–875. <https://doi.org/10.1016/j.epsl.2005.10.036>.
- Balescu, S., Lamothe, M., Mercier, N., Huot, S., Balteanu, D., Billard, A., Hus, J., 2003. Luminescence chronology of Pleistocene loess deposits from Romania: testing methods of age correction for anomalous fading in alkali feldspars. *Quat. Sci. Rev.* 22, 967–973. [https://doi.org/10.1016/S0277-3791\(03\)00056-8](https://doi.org/10.1016/S0277-3791(03)00056-8).
- Basarin, B., Bugge, B., Hambach, U., Marković, S.B., O'Hara-Dhand, K., Kovačević, A., Stevens, T., Guo, Z.T., Lukić, T., 2014. Time-scale and astronomical forcing of Serbian loess–paleosol sequences. *Global Planet. Change* 122, 89–106. <https://doi.org/10.1016/j.gloplacha.2014.08.007>.
- Baumgartner, M., Kindler, P., Eicher, O., Floch, G., Schilt, A., Schwander, J., Spahni, R., Capron, E., Chappellaz, J., Leuenberger, M., Fischer, H., Stocker, T.F., 2014. NGRIP CH₄ concentration from 120 to 10 kyr before present and its relation to a $\delta^{15}\text{N}$ temperature reconstruction from the same ice core. *Clim. Past* 10, 903–920. <https://doi.org/10.5194/cp-10-903-2014>.
- Blaauw, M., Wohlfarth, B., Andrés Christen, J., Ampel, L., Veres, D., Hugen, K.A., Preusser, F., Svensson, A., 2010. Were last glacial climate events simultaneous between Greenland and France? A quantitative comparison using non-tuned chronologies. *J. Quat. Sci.* 25, 387–394. <https://doi.org/10.1002/jqs.1330>.
- Bokhorst, M., Vandenbergh, J., Sümegi, P., Lanzoni, M., Gerasimenko, N.P., Matviishina, Zh., Marković, S., Frechen, M., 2011. Atmospheric circulation patterns in central and eastern Europe during the Weichselian pleniglacial inferred from loess grain-size record. *Quat. Int.* 234, 62–74. <https://doi.org/10.1016/j.quaint.2010.07.018>.
- Bugge, B., Glaser, B., Zöller, L., Hambach, U., Marković, S., Glaser, I., Gerasimenko, N., 2008. Geochemical characterization and origin of southeastern and eastern European loesses (Serbia, Romania, Ukraine). *Quat. Sci. Rev.* 27, 1058–1075. <https://doi.org/10.1016/j.quascirev.2008.01.018>.
- Bugge, B., Hambach, U., Glaser, B., Gerasimenko, N., Marković, S., Glaser, I., Zöller, L., 2009. Stratigraphy, and spatial and temporal paleoclimatic trends in South-eastern/Eastern European loess–paleosol sequences. *Quat. Int.* 196, 86–106. <https://doi.org/10.1016/j.quaint.2008.07.013>.
- Bugge, B., Hambach, U., Kehl, M., Marković, S.B., Zöller, L., Glaser, B., 2013. The progressive evolution of a continental climate in SE-Central European lowlands during the Middle Pleistocene recorded in loess paleosol sequences. *Geology* 41, 771–774. <http://geology.gsapubs.org/content/41/7/771.abstract>.
- Buylaert, J.P., Murray, A.S., Vandenbergh, D., Vriend, M., De Corte, F., Van den haute, P., 2008. Optical dating of Chinese loess using sand-sized quartz: establishing a time frame for Late Pleistocene climate changes in the western part of the Chinese Loess Plateau. *Quat. Geochronol.* 3, 99–113.
- Buylaert, J.P., Thiel, C., Murray, A.S., Vandenbergh, D.A.G., Yi, S., Lu, H., 2011a. IRSL and post-IR IRSL residual doses recorded in modern dust samples from the Chinese Loess Plateau. *Geochronometria* 38, 432–440.
- Buylaert, J.P., Huot, S., Murray, A.S., Van den haute, P., 2011b. Infrared stimulated luminescence dating of an Eemian (MIS 5e) site in Denmark using K-feldspar. *Boreas* 40, 46–56.
- Buylaert, J.P., Jain, M., Murray, A.S., Thomsen, K.J., Thiel, C., Sohbaty, R., 2012. A robust feldspar luminescence dating method for Middle and Late Pleistocene sediments. *Boreas* 41, 435–451. <https://doi.org/10.1111/j.1502-3885.2012.00248.x>.
- Caspers, G., Freund, H., 2001. Vegetation and climate in the early- and pleniglacial in northern central Europe. *J. Quat. Sci.* 16, 31–48.
- Chapot, M.S., Roberts, H.M., Duller, G.A.T., Lai, Z.P., 2012. A comparison of natural- and laboratory-generated dose response curves for quartz optically stimulated luminescence signals from Chinese Loess. *Radiat. Meas.* 47, 1045–1052. <https://doi.org/10.1016/j.radmeas.2012.09.001>.
- Chlebovsky, R., Gozhik, P.F., Lindner, L., Lanczont, M., Wojtanovicz, J., 2003. Stratigraphy and sedimentology of the Bug loess (Pleistocene: upper vistulian) between Kiev and odessa. *Geol. Q.* 47, 261–268. <https://gq.pgi.gov.pl/article/download/7315/5965>.
- Constantin, D., Timar-Gabor, A., Veres, D., Begy, R., Cosma, C., 2012. SAR-OSL dating of different grain-sized quartz from a sedimentary section in southern Romania interbedding the Campanian Ignimbrite/Y5 ash layer. *Quat. Geochronol.* 10, 81–86. <https://doi.org/10.1016/j.quageo.2012.01.012>.
- Constantin, D., Begy, R., Vasiliniuc, S., Panaioiu, C., Necula, C., Codrea, V., Timar-Gabor, A., 2014. High-resolution OSL dating of the Costinești section (Dobrogea, SE Romania) using fine and coarse quartz. *Quat. Int.* 334–335, 20–29. <https://doi.org/10.1016/j.quaint.2013.06.016>.
- Cunningham, A.C., Wallinga, J., 2010. Selection of integration time intervals for quartz OSL decay curves. *Quat. Geochronol.* 5, 657–666.
- Damblon, F., Haesaerts, P., Van der Plicht, J., 1996. New datings and considerations on the chronology of upper palaeolithic sites in the great eurasiatic plain. *Préhist. Europ.* 9, 177–231.
- De Vleeschouwer, D., Parnell, A., 2014. Reducing time scale uncertainty for the Devonian by integrating astrochronology and Bayesian statistics. *Geology* 42, 491–494. <https://doi.org/10.1130/G35618.1>.
- Delmonte, B., Basile-Doelsch, I., Petit, J.R., Maggi, V., Revel-Rolland, M., Michard, A., Jagoutz, E., Grousset, F., 2004. Comparing the Epica and Vostok dust records during the last 220,000 years: stratigraphical correlation and provenance in glacial periods. *Earth Sci. Rev.* 66, 63–87. <https://doi.org/10.1016/j.earscirev.2003.10.004>.
- Ding, Z.L., Derbyshire, E., Yang, S.L., Yu, Z.W., Xiong, S.F., Liu, T.S., 2002. Stacked 2.6-Ma grain size record from the Chinese loess based on five sections and correlation with the deep-sea $\delta^{18}\text{O}$ record. *Paleocean. Paleoclim.* 17, 1–21. <https://doi.org/10.1029/2001PA000725>.
- Duller, G.A.T., 2003. Distinguishing quartz and feldspar in single grain luminescence measurements. *Radiat. Meas.* 37, 161–165. [https://doi.org/10.1016/S1350-4487\(02\)00170-1](https://doi.org/10.1016/S1350-4487(02)00170-1).
- Evans, M.E., Rutter, N.W., Catto, N., Chlachula, J., Nyvlt, D., 2003. Magneto-climatology: teleconnection between the Siberian loess record and North Atlantic Heinrich events. *Geology* 31, 537–540. [https://doi.org/10.1130/0091-7613\(2003\)0312.0.CO;2](https://doi.org/10.1130/0091-7613(2003)0312.0.CO;2).
- Fischer, H., Behrens, M., Bock, M., Richter, U., Schmitt, J., Loulergue, L., Chappellaz, J., Spahni, R., Blunier, T., Leuenberger, M., Stocker, T.F., 2008. Changing boreal methane sources and constant biomass burning during the last termination. *Nature* 452, 864–867. <https://doi.org/10.1038/nature06825>.
- Fischer, P., Hambach, U., Klases, N., Schulte, P., Zeeden, C., Steininger, F., Lehmküh, F., Gerlach, R., Radtke, U., 2018. Landscape instability at the end of MIS 3 in western Central Europe: evidence from a multi proxy study on a Loess-Paleosol-Sequence from the eastern Lower Rhine Embayment, Germany. *Quat. Int.* (in press) <https://doi.org/10.1016/j.quaint.2017.09.008>.
- Fitzsimmons, K.E., Hambach, U., 2014. Loess accumulation during the last glacial maximum: evidence from Urluia, southeastern Romania. *Quat. Int.* 334–335, 74–85. <https://doi.org/10.1016/j.quaint.2013.08.005>.
- Fitzsimmons, K.E., Marković, S.B., Hambach, U., 2012. Pleistocene environmental dynamics recorded in the loess of the middle and lower Danube basin. *Quat. Sci. Rev.* 41, 104–118. <https://doi.org/10.1016/j.quascirev.2012.03.002>.
- Fitzsimmons, K.E., Hambach, U., Veres, D., Iovita, R., 2013. The campanian ignimbrite eruption: new data on volcanic ash dispersal and its potential impact on human evolution. *PLoS One* 8. <https://doi.org/10.1371/journal.pone.0065839>.
- Fleitmann, D., Cheng, H., Badertscher, S., Edwards, R.L., Mudelsee, M., Göktürk, O.M., Fankhäuser, A., Pickering, R., Raible, C.C., Matter, A., Kramers, J., Tüysüz, O., 2009. Timing and climatic impact of Greenland interstadials recorded in stalagmites from northern Turkey. *Geophys. Res. Lett.* 36, L19707. <https://doi.org/10.1029/2009GL040050>.
- Fletcher, W.J., Sánchez Goñi, M.F., Allen, J.R.M., Cheddadi, R., Combourieu-Nebout, N., Huntley, B., Lawson, I., Londeix, L., Magri, D., Margari, V., Müller, U.C., Naughton, F., Novenko, E., Roucoux, K., Tzedakis, P.C., 2010. Millennial-scale variability during the last glacial in vegetation records from Europe. *Quat. Sci. Rev.* 29, 2839–2864. <https://doi.org/10.1016/j.quascirev.2009.11.015>.
- Fu, X., Li, S.-H., 2013. A modified multi-elevated-temperature post IR-IRSL protocol for dating Holocene sediments using K-feldspar. *Quat. Geochronol.* 17, 44–54. <https://doi.org/10.1016/j.quageo.2013.02.004>.
- Fuchs, M., Kreutzer, S., Rousseau, D.D., Antoine, P., Hatté, C., Lagroix, F., Moine, O., Gauthier, C., Svoboda, J., Lisa, L., 2013. The loess sequence of dolni vestonice, Czech Republic: a new OSL-based chronology of the last climatic cycle. *Boreas* 42, 664–677. <https://doi.org/10.1111/j.1502-3885.2012.00299.x>.
- Gerasimenko, N., 2006. Late Pleistocene loess-paleosol and vegetational successions in the middle dnieper area, Ukraine. *Quat. Int.* 149, 55–66. <https://doi.org/10.1016/j.quaint.2005.11.018>.
- Gerasimenko, N.P., 2010. Korelyatsia korotkoperiodychnykh etapiv pleistotsenu za paleolandshaftnyimi dannymi. In: *Prostorovo-chasova Korelyatsia Paleogeografichnyh Umov Chetvertynnoho Periodu Na Teritorii Ukrainy*. Zh. M. Matviishina. Naukova dumka, Kyiv, pp. 104–129 (in Ukrainian).

- Gerasimenko, N., Rousseau, D.-D., 2008. Stratigraphy and paleoenvironments of the last pleniglacial in the Kyiv loess region (Ukraine). *Quaternaire* 19, 293–307. <http://quaternaire.revues.org/4592>.
- Giosan, L., Naing, T., Tun, M.M., Clift, D.P., Filip, F., Constantinescu, S., Khonde, N., Blusztajn, J., Buylaert, J.-P., Stevens, T., Thwin, S., 2018. On the Holocene evolution of the Ayeyawady megadelta. *Earth Surf. Dynam.* 6, 451–466. <https://doi.org/10.5194/esurf-6-451-2018>.
- Gocke, M., Hambach, U., Eckmeier, E., Schwark, L., Zöller, L., Fuchs, M., Löscher, M., Wiesenberg, G.L.B., 2014. Introducing an improved multi-proxy approach for paleoenvironmental reconstruction of loess–paleosol archives applied on the Late Pleistocene Nussloch sequence (SW Germany). *Palaeogeogr. Palaeoclimatol. Palaeoecol.* 410, 300–315. <https://doi.org/10.1016/j.palaeo.2014.06.006>.
- Govin, A., Capron, E., Tzedakis, P.C., Verheyden, S., Ghaleb, B., Hillaire-Marcel, C., St-Onge, G., Stoner, J.S., Bassinot, F., Bazin, L., Blunier, T., Combourieu-Nebout, N., El Ouahabi, A., Genty, D., Gersonde, R., Jimenez-Amat, P., Landais, A., Martrat, B., Masson-Delmotte, V., Parrenin, F., Seidenkrantz, M.S., Veres, D., Waelbroeck, C., Zahn, R., 2015. Sequence of events from the onset to the demise of the Last Interglacial: evaluating strengths and limitations of chronologies used in climatic archives. *Quat. Sci. Rev.* 129, 1–36. <https://doi.org/10.1016/j.quascirev.2015.09.018>.
- Gozhik, P., Komar, M., Lančzont, M., Fedorovicz, S., Bogucki, A., Mroczek, P., Prylypko, S., Kusiak, J., 2014. Paleoenvironmental history of the middle dnierper area from the dnierper to weichselian glaciation: a case study of the Maxymivka loess profile. *Quat. Int.* 334–335, 94–111. <https://doi.org/10.1016/j.quaint.2013.11.037>.
- Guérin, G., Mercier, N., Adamiec, G., 2011. Dose-rate conversion factors: update. *Ancient TL* 29, 5–8.
- Guo, Z.T., Ruddiman, W.F., Hao, Q.Z., Wu, H.B., Qiao, Y.S., Zhu, R.X., Peng, S.Z., Wei, J.J., Yuan, B.Y., Liu, T.S., 2002. Onset of Asian desertification by 22 Myr ago inferred from loess deposits in China. *Nature* 416, 159–163. <https://doi.org/10.1038/416159a>.
- Haase, D., Fink, J., Haase, G., Ruske, R., Pécsi, M., Richter, H., Altermann, M., Jäger, K.-D., 2007. Loess in Europe - its spatial distribution based on a european loess Map, 1:2500000. *Quat. Sci. Rev.* 26, 1301–1312. <https://doi.org/10.1016/j.quascirev.2007.02.003>.
- Haesaerts, P., Mestdagh, H., 2000. Pedosedimentary evolution of the last interglacial and early glacial sequence in the European loess belt from Belgium to central Russia. *Neth. J. Geosci.* 79, 313–324. <https://doi.org/10.1017/S001677460002179X>.
- Haesaerts, P., Borziac, I., Chekha, V.P., Chirica, V., Drozdov, N.I., Koulakovska, L., Orlova, L.A., van der Plicht, J., Damblon, F., 2010. Charcoal and wood remains for radiocarbon dating upper Pleistocene loess sequences in eastern Europe and central Siberia. *Palaeogeogr. Palaeoclimatol. Palaeoecol.* 291, 106–127, 2010. <https://doi.org/10.1016/j.palaeo.2010.03.034>.
- Haesaerts, P., Damblon, F., Gerasimenko, N., Spagna, P., Pirson, S., 2016. The Late Pleistocene loess–paleosol sequence of Middle Belgium. *Quat. Int.* 411, 25–43. <https://doi.org/10.1016/j.quaint.2016.02.012>.
- Hansen, V., Murray, A., Buylaert, J.-P., Yeo, E.-Y., Thomsen, K., 2015. A new irradiated quartz for beta source calibration. *Radiat. Meas.* 81, 123–127. <https://www.sciencedirect.com/science/article/abs/pii/S135044871500044X>.
- Hao, Q.Z., Wang, L., Oldfield, F., Peng, S.Z., Qin, L., Song, Y., Xu, B., Qiao, Y., Bloemendal, J., Guo, Z.T., 2012. Delayed build-up of Arctic ice sheets during 400,000-year minima in insolation variability. *Nature* 490, 393–396. <https://doi.org/10.1038/nature11493>.
- Hatté, C., Gauthier, C., Rousseau, D.D., Antoine, P., Fuchs, M., Lagroix, F., Marković, S.B., Moine, O., Sima, A., 2013. Excursions to C₄ vegetation recorded in the Upper Pleistocene loess of Surduk (Northern Serbia): an organic isotope geochemistry study. *Clim. Past* 9, 1001–1014. <http://www.clim-past.net/9/1001/2013/>.
- Heller, F., Liu, T., 1982. Magnetostratigraphical dating of loess deposits in China. *Nature* 300, 431–433.
- Hošek, J., Hambach, U., Lisá, L., Grygar, T.M., Horáček, I., Meszner, S., Knésl, I., 2015. An integrated rock-magnetic and geochemical approach to loess/paleosol sequences from Bohemia and Moravia (Czech Republic): implications for the Upper Pleistocene paleoenvironment in central Europe. *Palaeogeogr. Palaeoclimatol. Palaeoecol.* 418, 344–358. <https://doi.org/10.1016/j.palaeo.2014.11.024>.
- Huntley, D.J., Lamothe, M., 2001. Ubiquity of anomalous fading in K-feldspars and the measurement and correction for it in optical dating. *Can. J. Earth Sci.* 38, 1093–1106.
- Ivanov, I.V., Chendev, Y.G., 2015. Evolyutsia pochv lesostepi i chernozemnoy stepi tsentral'noy oblasti. In: Kudryarov, V.N., Ivanov, I.V. (Eds.), *Evolyutsia Pochv I Pochvennogo Pokrova*. GEOS, Moscow, pp. 456–469 (in Russian).
- Jary, Z., Ciszek, D., 2013. Late Pleistocene loess–paleosol sequences in Poland and western Ukraine. *Quat. Int.* 296, 37–50. <https://doi.org/10.1016/j.quaint.2012.07.009>.
- Kadereit, A., Wagner, G., 2014. Geochronological reconsideration of the eastern European key loess section at Stayky in Ukraine. *Clim. Past* 10, 783–796. <http://www.clim-past.net/10/783/2014/>.
- Kadereit, A., Kind, C.-J., Wagner, G.A., 2013. The chronological position of the Lohne Soil in the Nussloch loess section - re-evaluation for a European loess-marker horizon. *Quat. Sci. Rev.* 59, 67–86. <https://doi.org/10.1016/j.quascirev.2012.10.026>.
- Karmazinenko, S.P., 2010. Mikromorfologichni Doslidzennya Vykopnyh I Sychasnyh Gruntiv Ukrainy. *Naukova dumka, Kyiv (in Ukrainian)*.
- Kindler, P., Guillevic, M., Baumgartner, M., Schwander, J., Landais, A., Leuenberger, M., 2014. Temperature reconstruction from 10 to 120 kyr b2k from the NGRIP ice core. *Clim. Past* 10, 887–902. <https://www.clim-past.net/10/887/2014/>.
- Kohfeld, K.E., 2003. Glacial-interglacial changes in dust deposition on the Chinese Loess Plateau. *Quat. Sci. Rev.* 22, 1859–1878. [https://doi.org/10.1016/S0277-3791\(03\)00166-5](https://doi.org/10.1016/S0277-3791(03)00166-5).
- Kukla, G.J., 1977. Pleistocene land-sea correlations. I. Europe. *Earth Sci. Rev.* 13, 307–374. [https://doi.org/10.1016/0012-8252\(77\)90125-8](https://doi.org/10.1016/0012-8252(77)90125-8).
- Kunitsa, N.I., 2007. *Priroda Ukrainy V Pleistotsene (Po Dannym Malacologicheskogo Analiza)*. Ruta, Chernovtsy (in Russian).
- Kusiak, J., Lančzont, M., Bogucki, A., 2012. New exposure of loess deposits in Boyanichi (Ukraine) - results of thermoluminescence analyses. *Geochronique* 39, 84–100. <https://doi.org/10.2478/s13386-011-0054-1>.
- Lančzont, M., Madeyska, T., Bogucki, A., Sytnyk, O., Kusiak, J., Frankowski, Z., Komar, M., Nawrocki, J., Żogała, B., 2014. Stratigraphic position and natural environment of the oldest Middle Palaeolithic in central Podolia, Ukraine: new data from the Velykyi Glybochok site. *Quat. Int.* 326–327, 191–212. <https://doi.org/10.1016/j.quaint.2013.08.045>.
- Labaz, B., Muszytyfaga, E., Waroszewski, J., Bogacz, A., Jezierski, P., Kabala, C., 2018. Landscape-related transformation and differentiation of chernozems - catenary approach in the silesian lowland, SW Poland. *Catena* 161, 63–76. <https://doi.org/10.1016/j.catena.2017.10.003>.
- Lai, Z.P., 2010. Chronology and the upper dating limit for loess samples from Luochuan section in the Chinese Loess Plateau using quartz OSL SAR protocol. *J. Asian Earth Sci.* 37, 176–185. <https://doi.org/10.1016/j.jseae.2009.08.003>.
- Lai, Z.-P., Fan, A.C., 2013. Examining quartz OSL age underestimation for loess samples from Luochuan in the Chinese Loess Plateau. *Geochronometria* 41, 57–64. <https://doi.org/10.2478/s13386-013-0138-1>.
- Lang, N., Wolff, E.W., 2011. Interglacial and glacial variability from the last 800 ka in marine, ice and terrestrial archives. *Clim. Past* 7, 361–380. <http://www.clim-past.net/7/361/2011/>.
- Lehmkuhl, F., Zens, J., Krauß, L., Schulte, P., Kels, H., 2016. Loess-paleosol sequences at the northern European loess belt in Germany: distribution, geomorphology and stratigraphy. *Quat. Sci. Rev.* 153, 11–30. <https://doi.org/10.1016/j.quascirev.2016.10.008>.
- Li, B., Li, S.H., 2011. Luminescence dating of K-feldspar from sediments: a protocol without anomalous fading correction. *Quat. Geochronol.* 6, 468–479.
- Lindner, L., Bogucki, A., Gozhik, P., Marks, L., Lančzont, M., Wojtanowicz, J., 2006. Correlation of the Pleistocene deposits in the area between the Baltic and Black Sea, central Europe. *Geol. Q.* 50, 195–210. <https://gq.pgi.gov.pl/article/view/7405>.
- Lisá, L., Neruda, P., Nerudová, Z., Nejman, L., 2018. Podhradem interstadial; a critical review of the middle and late MIS 3 (denekamp, hengelo) in Moravia, Czech Republic. *Quat. Sci. Rev.* 182, 191–201. <https://doi.org/10.1016/j.quascirev.2017.12.024>.
- Lisiecki, L.E., Raymo, M.E., 2005. A Pliocene-Pleistocene stack of 57 globally distributed benthic $\delta^{18}\text{O}$ records. *Paleoceanography* 20, PA1003. <https://doi.org/10.1029/2004PA001071>.
- Longman, J., Veres, D., Ersek, V., Salzmann, U., Hubay, K., Bormann, M., Wennrich, V., Schäbitz, F., 2017. Periodic input of dust over the Eastern Carpathians during the Holocene linked with Saharan desertification and human impact. *Clim. Past* 13, 897–917. <https://doi.org/10.5194/cp-13-897-2017>.
- Lowick, S.E., Preusser, F., 2011. Investigating age underestimation in the high dose region of optically stimulated luminescence using fine grain quartz. *Quat. Geochronol.* 6, 33–41. <https://doi.org/10.1016/j.quageo.2010.08.001>.
- Lowick, S.E., Preusser, F., Pini, R., Ravazzi, C., 2010. Underestimation of fine grain quartz OSL dating towards the Eemian: comparison with palynostratigraphy from Azzano Decimo, northeastern Italy. *Quat. Geochronol.* 5, 583–590. <https://doi.org/10.1016/j.quageo.2009.12.003>.
- Luetscher, M., Boch, R., Sodemann, H., Spötl, C., Cheng, H., Edwards, R.L., Frisia, S., Hof, F., Müller, W., 2015. North Atlantic storm track changes during the last glacial maximum recorded by alpine speleothems. *Nat. Commun.* 6, 6344. <https://doi.org/10.1038/ncomms7344>.
- Magyari, E.K., Veres, D., Wennrich, V., Wagner, B., Braun, M., Jakab, G., Karátson, D., Pál, Z., Ferenczy, G., St-Onge, G., Rethemeyer, J., Francois, J.-P., von Reumont, F., Schäbitz, F., 2014. Vegetation and environmental responses to climate forcing during the Last Glacial Maximum and deglaciation in the East Carpathians: attenuated response to maximum cooling and increased biomass burning. *Quat. Sci. Rev.* 106, 278–298. <https://doi.org/10.1016/j.quascirev.2014.09.015>.
- Maher, B.A., Prospero, J.M., Mackie, D., Gaiero, D., Hesse, P.P., Balkanski, Y., 2010. Global connections between aeolian dust, climate and ocean biogeochemistry at the present day and at the last glacial maximum. *Earth Sci. Rev.* 99, 61–97. <https://doi.org/10.1016/j.earscirev.2009.12.001>.
- Marković, S.B., Hambach, U., Stevens, T., Kukla, G.J., Heller, F., McCoy, W.D., Oches, E.A., Buggie, B., Zöller, L., 2011. The last million years recorded at the Stari Slankamen loess–paleosol sequence: revised chronostratigraphy and long-term environmental trends. *Quat. Sci. Rev.* 30, 1142–1154. <https://doi.org/10.1016/j.quascirev.2011.02.004>.
- Marković, S.B., Stevens, T., Kukla, G.J., Hambach, U., Fitzsimmons, K.E., Gibbard, P., Buggie, B., Zech, M., Guo, Z., Hao, Q., Wu, H., O'Hara Dhand, K., Smalley, I.J., Újvári, G., Sümegi, P., Timar-Gabor, A., Veres, D., Sirocko, F., Vasiljev, D.A., Jary, Z., Svensson, A., Jović, V., Lehmkuhl, F., Kovács, J., Svirčev, Z., 2015. Danube loess stratigraphy – towards a pan-European loess stratigraphic model. *Earth*

- Sci. Rev. 148, 228–258. <https://doi.org/10.1016/j.earscrev.2015.06.005>.
- Matoshko, A.V., 1999. Sedimentary model of the Staiky loess plateau, Pridniprovs'ka Upland, Ukraine. *Geol. Q.* 43, 219–232.
- Matviishina, Zh.N., Gerasimenko, N.P., Perederiy, V.I., Ivchenko, A.S., Parchomenko, O.G., Karmazinenko, S.P., 2010. Prostorovo-chasova Korelyatsia Paleogeografichnyh Umov Chetvertynnoho Periodu Na Territorii Ukrainy. *Naukova dumka, Kyiv*, p. 2010 (in Ukrainian).
- Mejdahl, V., 1979. Thermoluminescence dating: beta-dose attenuation in quartz grains. *Archaeometry* 21, 61–72. <https://doi.org/10.1111/j.1475-4754.1979.tb00241.x>.
- Ménot, G., Bard, E., 2012. A precise search for drastic temperature shifts of the past 40,000 years in southeastern Europe. *Paleoceanography* 27, PA2210. <https://doi.org/10.1029/2012PA002291>.
- Ménot, G., Bard, E., Rostek, F., Weijers, J.W.H., Hopmans, E.C., Schouten, S., Damsté, J.S.S., 2006. Early reactivation of European rivers during the last deglaciation. *Science* 313, 1623–1625. <https://doi.org/10.1126/science.1130511>.
- Mesner, S., Kreutzer, S., Fuchs, M., Faust, D., 2013. Late Pleistocene landscape dynamics in Saxony, Germany: paleoenvironmental reconstruction using loess-paleosol sequences. *Quat. Int.* 296, 94–107. <https://doi.org/10.1016/j.quaint.2012.12.040>.
- Moine, O., Antoine, P., Hatté, C., Landais, A., Mathieu, J., Prud'homme, C., Rousseau, D.-D., 2017. The impact of Last Glacial climate variability in west-European loess revealed by radiocarbon dating of fossil earthworm granules. *Proc. Natl. Acad. Sci. Unit. States Am.* 114, 6209–6214. <http://www.pnas.org/content/early/2017/05/23/1614751114.abstract>.
- Moreno, A., Stoll, H.M., Jiménez-Sánchez, M., Cacho, I., Valero-Garcés, B., Ito, E., Edwards, L.R., 2010. A speleothem record of rapid climatic shifts during last glacial period from Northern Iberian Peninsula. *Global Planet. Change* 71, 218–231. <https://doi.org/10.1016/j.gloplacha.2009.10.002>.
- Murray, A.S., Wintle, A.G., 2000. Luminescence dating of quartz using an improved single-aliquot regenerative-dose protocol. *Radiat. Meas.* 32, 57–73. [https://doi.org/10.1016/S1350-4487\(99\)00253-X](https://doi.org/10.1016/S1350-4487(99)00253-X).
- Murray, A.S., Wintle, A.G., 2003. The single aliquot regenerative dose protocol: potential for improvements in reliability. *Radiat. Meas.* 37, 377–381. [https://doi.org/10.1016/S1350-4487\(03\)00053-2](https://doi.org/10.1016/S1350-4487(03)00053-2).
- Murray, A.S., Svendsen, J.I., Mangerud, J., Astakhov, V.I., 2007. Testing the accuracy of quartz OSL dating using a known-age Eemian site on the river Sula, northern Russia. *Quat. Geochronol.* 2, 107–109. <https://doi.org/10.1016/j.quageo.2006.04.004>.
- Murray, A.S., Schmidt, E.D., Stevens, T., Buylaert, J.P., Markovic, S., Tsukamoto, S., Frechen, M., 2014. Dating middle pleistocene loess from stari slankamen (Vojvodina, Serbia) - limitations imposed by the saturation behaviour of an elevated temperature IRSL signal. *Catena* 117, 34–42. <https://www.sciencedirect.com/science/article/pii/S0341816213001689>.
- Naafs, B.D.A., Hefter, J., Grützer, J., Stein, R., 2013. Warming of surface waters in the mid-latitude North Atlantic during the Steiner Heinrich events. *Paleoceanography* 28, 153–163. <https://doi.org/10.1029/2012PA002354>.
- Nawrocki, J., Bakhmutov, V., Bogucki, A., Dolecki, L., 1999. The paleo- and petromagnetic record in the Polish and Ukrainian loess-paleosol sequences. *Phys. Chem. Earth Solid Earth Geodes.* 24, 773–777. [https://doi.org/10.1016/S1464-1895\(99\)00113-1](https://doi.org/10.1016/S1464-1895(99)00113-1).
- Obrecht, I., Zeeden, C., Hambach, U., Veres, D., Marković, S.B., Bösen, J., Svirčev, Z., Bačević, N., Gavrilov, M.B., Lehmkühl, F., 2016. Tracing the influence of Mediterranean climate on Southeastern Europe during the past 350,000 years. *Sci. Rep.* 6, 36334. <https://doi.org/10.1038/srep36334>.
- Obrecht, I., Hambach, U., Veres, D., Zeeden, C., Bösen, J., Stevens, T., Marković, S.B., Klagen, N., Brill, D., Burrow, C., Lehmkühl, F., 2017. Shift of large-scale atmospheric systems over Europe during late MIS 3 and implications for Modern Human dispersal. *Sci. Rep.* 7, 5848. <https://doi.org/10.1038/s41598-017-06285-x>.
- Panaiotu, C.G., Panaiotu, C.E., Grama, A., Necula, C., 2001. Paleoclimatic record from a loess-paleosol profile in southeastern Romania. *Phys. Chem. Earth A* 26, 893–898. [https://doi.org/10.1016/S1464-1895\(01\)00138-7](https://doi.org/10.1016/S1464-1895(01)00138-7).
- Prescott, J.R., Hutton, J.T., 1994. Cosmic ray contributions to dose rates for luminescence and ESR dating: large depths and long term variations. *Radiat. Meas.* 23, 497–500. [https://doi.org/10.1016/1350-4487\(94\)90086-8](https://doi.org/10.1016/1350-4487(94)90086-8).
- Rasmussen, S.O., Bigler, M., Blockley, S.P., Blunier, T., Buchardt, S.L., Clausen, H.B., Cvijanovic, I., Dahl-Jensen, D., Johnsen, S.J., Fischer, H., Gkinis, V., Guillevic, M., Hoek, W.Z., Lowe, J.J., Pedro, J.B., Popp, T., Seierstad, I.K., Steffensen, J.P., Svensson, A.M., Vallelonga, P., Vinther, B.M., Walker, M.J.C., Wheatley, J.J., Winstrup, M., 2014. A stratigraphic framework for abrupt climatic changes during the Last Glacial period based on three synchronized Greenland ice-core records: refining and extending the INTIMATE event stratigraphy. *Quat. Sci. Rev.* 106, 14–28. <https://doi.org/10.1016/j.quascirev.2014.09.007>.
- Rees-Jones, J., 1995. Optical dating of young sediments using fine-grain quartz. *Ancient TL* 13, 9–13.
- Roberts, H.M., 2008. The development and application of luminescence dating to loess deposits: a perspective on the past, present and future. *Boreas* 37, 483–507. <http://onlinelibrary.wiley.com/doi/10.1111/j.1502-3885.2008.00057.x/full>.
- Roberts, H.M., 2012. Testing Post-IR IRSL protocols for minimising fading in feldspars, using Alaskan loess with independent chronological control. *Radiat. Meas.* 47, 716–724. <https://doi.org/10.1016/j.radmeas.2012.03.022>.
- Rostek, F., Bard, E., 2013. Hydrological changes in eastern Europe during the last 40,000 yr inferred from biomarkers in Black Sea sediments. *Quat. Res.* 80, 502–509. <https://doi.org/10.1016/j.yqres.2013.07.003>.
- Rousseau, D.-D., Gerasimenko, N., Matviishina, Zh., Kukla, G., 2001. Late Pleistocene environments of Central Ukraine. *Quat. Res.* 56, 349–356. <https://doi.org/10.1006/qres.2001.2270>.
- Rousseau, D.-D., Sima, A., Antoine, P., Hatté, C., Lang, A., Zöller, L., 2007. Link between European and North Atlantic abrupt climate changes over the last glaciation. *Geophys. Res. Lett.* 34, L22713. <https://doi.org/10.1029/2007GL031716>.
- Rousseau, D.-D., Antoine, P., Gerasimenko, N., Sima, A., Fuchs, M., Hatté, C., Moine, O., Zoeller, L., 2011. North Atlantic abrupt climatic events of the last glacial period recorded in Ukrainian loess deposits. *Clim. Past* 7, 221–234. <http://www.clim-past.net/7/221/2011/>.
- Rousseau, D.-D., Svensson, A., Bigler, M., Sima, A., Steffensen, J.P., Boers, N., 2017a. Eurasian contribution to the last glacial dust cycle: how are loess sequences built? *Clim. Past* 13, 1181–1197. <https://doi.org/10.5194/cp-13-1181-2017>.
- Rousseau, D.-D., Boers, N., Sima, A., Svensson, A., Bigler, M., Lagroix, F., Taylor, S., Antoine, P., 2017b. (MIS3 & 2) millennial oscillations in Greenland dust and Eurasian aeolian records – a paleosol perspective. *Quat. Sci. Rev.* 169, 99–113. <https://doi.org/10.1016/j.quascirev.2017.05.020>.
- Ruth, U., Bigler, M., Röthlisberger, R., Siggaard-Andersen, M.-L., Kipfthuhl, S., Goto-Azuma, K., Hansson, M.E., Johnsen, S.J., Lu, H., Steffensen, J.P., 2007. Ice core evidence for a very tight link between North Atlantic and east Asian glacial climate. *Geophys. Res. Lett.* 34, L03706. <https://doi.org/10.1029/2006GL027876>.
- Sanchez Goñi, M.F., Harrison, S.P., 2010. Millennial-scale climate variability and vegetation changes during the Last Glacial: concepts and terminology. *Quat. Sci. Rev.* 29, 2823–2827. <https://doi.org/10.1016/j.quascirev.2009.11.014>.
- Sauer, D., Kadereit, A., Kühn, P., Kösel, M., Miller, E.C., Shinonaga, T., Kreutzer, S., Herrmann, L., Fleck, W., Starkovich, B.M., Stahr, K., 2016. The loess-paleosol sequence of Datthausen, SW Germany: characteristics, chronology, and implications for the use of the Lohne Soil as a marker soil. *Catena* 146, 10–29. <https://doi.org/10.1016/j.catena.2016.06.024>.
- Shi, C., Zhu, R., Glass, B.P., Liu, Q., Zeman, A., Suchy, V., 2003. Climate variations since the last interglacial recorded in Czech loess. *Geophys. Res. Lett.* 30, 1562. <https://doi.org/10.1029/2003GL017251>.
- Shumilovskikh, L.S., Fleitmann, D., Nowaczyk, N.R., Behling, H., Marret, F., Wegwerth, A., Arz, H.W., 2014. Orbital- and millennial-scale environmental changes between 64 and 20 ka BP recorded in Black Sea sediments. *Clim. Past* 10, 939–954. <http://www.clim-past.net/10/939/2014/>.
- Sima, A., Kageyama, M., Rousseau, D.-D., Ramstein, G., Balkanski, Y., Antoine, P., Hatté, C., 2013. Modeling dust emission during the North Atlantic millennial-scale climate variations from the perspective of East Europe MIS 3 loess deposits. *Clim. Past* 9, 1385–1402. <https://doi.org/10.5194/cp-9-1385-2013>.
- Sirocko, F., Knapp, H., Dreher, F., Förster, M.W., Albert, J., Brunuck, H., Veres, D., Dietrich, S., Zech, M., Hambach, U., Röhrer, M., Rudert, S., Schwibus, K., Adams, C., Sigl, P., 2016. The ELSA-Vegetation-Stack: reconstruction of Landscape Evolution Zones (LEZ) from laminated Eifel maar sediments of the last 60,000 years. *Global Planet. Change* 142, 108–135. <https://doi.org/10.1016/j.gloplacha.2016.03.005>.
- Sprafke, T., Obrecht, I., 2016. Loess: rock, sediment or soil – what is missing for its definition? *Quat. Int.* 399, 198–207. <https://doi.org/10.1016/j.quaint.2015.03.033>.
- Stevens, T., Marković, S.B., Zech, M., Hambach, U., Sümege, P., 2011. Dust deposition and climate in the Carpathian Basin over an independently dated last glacial-interglacial cycle. *Quat. Sci. Rev.* 30, 662–681. <https://doi.org/10.1016/j.quascirev.2010.12.011>.
- Svensson, A., Andersen, K.K., Bigler, M., Clausen, H.B., Dahl-Jensen, D., Davies, S.M., Johnsen, S.J., Muscheler, R., Parrenin, F., Rasmussen, S.O., Röthlisberger, R., Seierstad, I., Steffensen, J.P., Vinther, B.M., 2008. A 60 000 year Greenland stratigraphic ice core chronology. *Clim. Past* 4, 47–57. <https://www.clim-past.net/4/47/2008/>.
- Terhorst, B., Kühn, P., Damm, B., Hambach, U., Meyer-Heintze, S., Sedov, S., 2014. Paleoenvironmental fluctuations as recorded in the loess-paleosol sequence of the Upper Paleolithic site Krems-Wachtberg. *Quat. Int.* 351, 67–82. <https://doi.org/10.1016/j.quaint.2013.03.045>.
- Thiel, C., Buylaert, J.P., Murray, A.S., Terhorst, B., Hofer, I., Tsukamoto, S., Frechen, M., 2011a. Luminescence dating of the Strating loess profile (Austria) – testing the potential of an elevated temperature post-IR IRSL protocol. *Quat. Int.* 234, 23–31. <https://www.sciencedirect.com/science/article/pii/S1040618210002156?via%3DIihub>.
- Thiel, C., Buylaert, J.P., Murray, A.S., Tsukamoto, S., 2011b. On the applicability of post-IR IRSL dating to Japanese loess. *Geochronometria* 38, 369–378.
- Thiel, C., Buylaert, J.P., Murray, A.S., Elmejdoub, N., 2012. A comparison of TT-OSL and post-IR IRSL dating of coastal deposits on Cap Bon peninsula, north-eastern Tunisia. *Quat. Geochronol.* 10, 209–217.
- Thomsen, K.J., Bøtter-Jensen, L., Denby, P.M., Moska, P., Murray, A.S., 2006. Developments in luminescence measurement techniques. *Radiat. Meas.* 41, 768–773. <https://doi.org/10.1016/j.radmeas.2006.06.010>.
- Thomsen, K.J., Murray, A.S., Jain, M., 2011. Stability of IRSL signals from sedimentary K-feldspar samples. *Geochronique* 38, 1–13. <https://www.degruyter.com/view/j/geochr.2011.38.issue-1/s13386-011-0003-z/s13386-011-0003-z.xml>.
- Timar, A., Vandenberghe, D., Panaiotu, E.C., Panaiotu, C.G., Necula, C., Cosma, C., van de haute, P., 2010. Optical dating of Romanian loess using fine-grained quartz. *Quat. Geochronol.* 5, 143–148. <https://doi.org/10.1016/j.quageo.2009.03.003>.
- Timar-Gabor, A., Wintle, A.G., 2013. On natural and laboratory generated dose response curves for quartz of different grain sizes from Romanian loess. *Quat.*

- Geochronol. 18, 34–40. <https://doi.org/10.1016/j.quageo.2013.08.001>.
- Timar-Gabor, A., Vandenberghe, D.A.G., Vasiliniuc, S., Panaiotu, C.E., Panaiotu, C.G., Dimofte, D., Cosma, C., 2011. Optical dating of Romania loess: a comparison between sand-sized and silt-sized quartz. *Quat. Int.* 240, 62–70. <https://doi.org/10.1016/j.quaint.2010.10.007>.
- Timar-Gabor, A., Vasiliniuc, S., Vandenberghe, D.A.G., Cosma, C., Wintle, A.G., 2012. Investigations into the reliability of SAR-OSL equivalent doses obtained for quartz samples displaying dose response curves with more than one component. *Radiat. Meas.* 47, 740–745, 2012. <https://doi.org/10.1016/j.radmeas.2011.12.001>.
- Timar-Gabor, A., Constantin, D., Marković, S.B., Jain, M., 2015. Extending the area of investigation of fine versus coarse quartz optical ages from the Lower Danube to the Carpathian Basin. *Quat. Int.* 388, 168–176. <https://doi.org/10.1016/j.quaint.2014.09.065>.
- Timar-Gabor, A., Buylaert, J.-P., Guralnik, B., Trandafir-Antohei, O., Constantin, D., Anechitei-Deacu, V., Jain, M., Murray, A.S., Porat, N., Hao, Q., Wintle, A.G., 2017. On the importance of grain size in luminescence dating using quartz. *Radiat. Meas.* 106, 464–471. <https://doi.org/10.1016/j.radmeas.2017.01.009>.
- Toucanne, S., Soulet, G., Freslon, N., Silva Jacinto, R., Dennielou, B., Zaragosi, S., Eynaud, F., Bourillet, J.-F., Bayon, G., 2015. Millennial-scale fluctuations of the European Ice Sheet at the end of the last glacial, and their potential impact on global climate. *Quat. Sci. Rev.* 123, 113–133. <https://doi.org/10.1016/j.quascirev.2015.06.010>.
- Trandafir, O., Timar-Gabor, A., Schmidt, C., Veres, D., Anghelinu, M., Hambach, U., Simon, S., 2015. OSL dating of fine and coarse quartz from a Palaeolithic sequence on the Bistrița Valley (Northeastern Romania). *Quat. Geochronol.* 30, 487–492. <https://doi.org/10.1016/j.quageo.2014.12.005>.
- Újvári, G., Kok, J.F., Varga, G., Kovács, J., 2016a. The physics of wind-blown loess: implications for grain size proxy interpretations in Quaternary paleoclimate studies. *Earth Sci. Rev.* 154, 247–278. <https://doi.org/10.1016/j.earscirev.2016.01.006>.
- Újvári, G., Molnár, M., Páll-Gergely, B., 2016b. Charcoal and mollusc shell ¹⁴C-dating of the Dunaszekcső loess record, Hungary. *Quat. Geochronol.* 35, 43–53. <https://doi.org/10.1016/j.quageo.2016.05.005>.
- Vandenberghe, J., 2000. A global perspective of the European chronostratigraphy for the past 650 ka. *Quat. Sci. Rev.* 19, 1701–1707. [https://doi.org/10.1016/S0277-3791\(00\)00096-2](https://doi.org/10.1016/S0277-3791(00)00096-2).
- Vandenberghe, J., van der Plicht, J., 2016. The age of the Hengelo interstadial revisited. *Quat. Geochronol.* 32, 21–28. <https://doi.org/10.1016/j.quageo.2015.12.004>.
- Vandenberghe, J., Coope, R., Kasse, K., 1998. Quantitative reconstructions of palaeoclimates during the last interglacial-glacial in western and central Europe: an introduction. *J. Quat. Sci.* 13, 361–366.
- Vandenberghe, D.A.G., De Corte, F., Buylaert, J.-P., Kučera, J., Van den haute, P., 2008. On the internal radioactivity in quartz. *Radiat. Meas.* 43, 771–775. <https://doi.org/10.1016/j.radmeas.2008.01.016>.
- Vandenberghe, J., Marković, S.B., Jovanović, M., Hambach, U., 2014. Site-specific variability of loess and palaeosols (Ruma, Vojvodina, northern Serbia). *Quat. Int.* 334–335, 86–93. <https://doi.org/10.1016/j.quaint.2013.10.036>.
- Vasiliniuc, Ș., Vandenberghe, D.A.G., Timar-Gabor, A., Panaiotu, C., Cosma, C., Van den haute, P., 2012. Testing the potential of elevated temperature post-IR-IRSL signals for dating Romanian loess. *Quat. Geochronol.* 10, 75–80. <https://doi.org/10.1016/j.quageo.2012.02.014>.
- Vasiliniuc, Ș., Vandenberghe, D.A.G., Timar-Gabor, A., Cosma, C., van den haute, P., 2013. Combined IRSL and POST-IR OSL dating of Romanian loess using single aliquots of polymineral fine grains. *Quat. Int.* 293, 15–22. <https://doi.org/10.1016/j.quaint.2012.01.002>.
- Veklich, M.F., 1968. Stratigrafia Lessovoy Formatsii Ukrainy I Sosednih Stran (Stratigraphy of Loess Series of Ukraine and the Adjacent Areas). *Naukova dumka, Kiev*.
- Veklich, M.F. (Ed.), 1993. *Stratigrafichesky Shema Chetvertichnyh Otlozheniy Ukrainy (Stratigraphical Framework of the Quaternary of Ukraine)*. Gosgeolkom Ukrainy, Kiev.
- Veklich, M.F., Sirenko, N.A., Matviishina, ZhN., Mel'nichuk, I.V., Nagirny, V.N., Perederiy, V.P., Turlo, S.I., Gerasimenko, N.P., Vozgrin, B.D., 1984. *Palaeogeografia Kievskogo Pridneprovya (Palaeogeography of the Kiev–Dnieper Area)*. *Naukova dumka, Kiev*.
- Veres, D., Lallier-Verges, E., Wohlfarth, B., Lacourse, T., Keravis, D., Björck, S., Preusser, F., Andrieu-Ponel, V., Ampel, L., 2009. Climate-driven changes in lake conditions during late MIS 3 and MIS 2: a high-resolution geochemical record from Les Echets, France. *Boreas* 38, 230–243. <https://doi.org/10.1111/j.1502-3885.2008.00066.x>.
- Veres, D., Bazin, L., Landais, A., Toyé Mahamadou Kele, H., Lemieux-Dudon, B., Parrenin, F., Martinerie, P., Blayo, E., Blunier, T., Capron, E., Chappellaz, J., Rasmussen, S.O., Severi, M., Svensson, A., Vinther, B., Wolff, E.W., 2013a. The Antarctic ice core chronology (AICC2012): an optimized multi-parameter and multi-site dating approach for the last 120 thousand years. *Clim. Past* 9, 1733–1748. <https://doi.org/10.5194/cp-9-1733-2013>.
- Veres, D., Lane, C.S., Timar-Gabor, A., Hambach, U., Constantin, D., Szakács, A., Fülling, A., Onac, B.P., 2013b. The Campanian Ignimbrite/Y5 tephra layer – a regional stratigraphic marker for Isotope Stage 3 deposits in the Lower Danube region, Romania. *Quat. Int.* 293, 22–33. <https://doi.org/10.1016/j.quaint.2012.02.042>.
- Wintle, A.G., 1973. Anomalous fading of thermoluminescence in mineral samples. *Nature* 245, 143–144.
- Wintle, A.G., Murray, A.S., 2006. A review of quartz optically stimulated luminescence characteristics and their relevance in single-aliquot regeneration dating protocols. *Radiat. Meas.* 41, 369–391. <https://doi.org/10.1016/j.radmeas.2005.11.001>.
- Wohlfarth, B., Veres, D., Ampel, L., Lacourse, T., Blaauw, M., Preusser, F., Andrieu-Ponel, V., Keravis, D., Lallier-Vergès, E., Björck, S., Davies, S.M., de Beaulieu, J.-L., Risberg, J., Hormes, A., Kasper, H.U., Possnert, G., Reille, M., Thouveny, N., Zander, A., 2008. Rapid ecosystem response to abrupt climate changes during the last glacial period in western Europe, 40–16 ka. *Geology* 36, 407–410. <https://doi.org/10.1130/G24600A.1>.
- Zech, M., Zech, R., Marković, S., Hambach, U., Huang, Y., 2013. Humid glacials, arid interglacials? Critical thoughts on pedogenesis and paleoclimate based on multi-proxy analyses of the loess-paleosol sequence Crvenka, Northern Serbia. *Palaeogeogr. Palaeoclimatol. Palaeoecol.* 387, 165–175. <https://doi.org/10.1016/j.palaeo.2013.07.023>.
- Zeeden, C., Kels, H., Hambach, U., Schulte, P., Protze, J., Eckmeier, E., Marković, S.B., Klasen, N., Lehmkuhl, F., 2016. Three climatic cycles recorded in a loess-paleosol sequence at Smeclac (Romania) – implications for dust accumulation in south-eastern Europe. *Quat. Sci. Rev.* 154, 130–142. <https://doi.org/10.1016/j.quascirev.2016.11.002>.
- Zeeden, C., Hambach, U., Obrecht, I., Hao, Q., Abels, H.A., Veres, D., Lehmkuhl, F., Gavrilov, M.B., Marković, S.B., 2018a. Patterns and timing of loess-paleosol transitions in Eurasia: constraints for paleoclimate studies. *Global Planet. Change* 162, 1–7. <https://doi.org/10.1016/j.gloplacha.2017.12.021>.
- Zeeden, C., Dietze, M., Kreutzer, S., 2018b. Discriminating luminescence age uncertainty composition for a robust Bayesian modelling. *Quat. Geochronol.* 43, 30–39. <https://doi.org/10.1016/j.quageo.2017.10.001>.
- Zeeden, C., Hambach, U., Veres, D., Fitzsimmons, K., Obrecht, I., Bösen, J., Lehmkuhl, F., 2018. Millennial scale climate oscillations recorded in the Lower Danube loess over the last glacial period. *Palaeogeogr. Palaeoclimatol. Palaeoecol.* (in press) <https://doi.org/10.1016/j.palaeo.2016.12.029>.